Cara M, Van der Woerd J, Alasset PJ, Benjumea J, Mériaux AS.

The 1905 Chamonix earthquakes: active tectonics in the Mont Blanc and Aiguilles Rouges massifs.

***Swiss Journal of Geosciences* 2017**

DOI: http://dx.doi.org/10.1007/s00015-017-0262-7

Title: The 1905 Chamonix earthquakes: active tectonics in the Mont Blanc and Aiguilles Rouges massifs

Authors: Michel Cara[1], Jérôme Van der Woerd[1], Pierre-Jean Alasset[2], Juan Benjumea[1], Anne-Sophie Mériaux[3]

[1] Université de Strasbourg, EOST-UMR7516, 5 rue R. Descartes, 67084 Strasbourg Cedex, France

[2] C-Core, 400 March Road, Suite 210 Ottawa, ON, Canada, K2K 3H4

[3] School of Geography, Politics and Sociology, Newcastle University, Newcastle upon Tyne, United Kingdom

Author for correspondence: Michel Cara, E-mail: michel.cara@unistra.fr

Keywords: Earthquake, Alps, Tectonics, Seismology

Abstract

Linking earthquakes of moderate size to known tectonic sources is a challenge for seismic hazard studies in northwestern Europe because of overall low strain rates. Here we present a combined study of macroseismic information, tectonic observations, and seismic waveform modelling to document the largest instrumentally known event in the French northern Alps, the April 29, 1905, Chamonix earthquake. The moment magnitude of this event is estimated at M_w5.3±0.3 from records in Göttingen (Germany) and Uppsala (Sweden). The event of April 29 was followed by several afterschocks and in particular a second broadly felt earthquake on August 13, 1905. Macroseismic investigations allow us to favour a location of the epicentres 5 to 10 km N-NE of Chamonix. Tectonic analysis shows that potentially one amongst several faults might have been activated in 1905. Among them the right lateral strike-slip fault responsible for the recent 2005 M_w = 4.4 Vallorcine earthquake and a quasi-normal fault northeast of the Aiguilles Rouges massif are the most likely candidates. Discussion of tectonic, macroseismic, and instrumental data favour the normal fault hypothesis for the 1905 Chamonix earthquake sequence.

1 Introduction

The northwestern Alps are one of the most seismically active regions of France and Switzerland. In the Valais canton, several earthquakes of magnitude ≈ 6 caused serious damages over the past

centuries (e.g. Fäh et al. 2012). Together with the Basel area, this is the region where seismic hazard is highest in Switzerland. Similarly in the new French seismic regulation code, the neighbouring Haute-Savoie is set at the highest seismic hazard level of metropolitan France (Plan-séisme 2015). These levels of seismic hazard are mainly estimated from statistical analysis of instrumental and historical seismicity. Due to a somewhat low to moderate seismicity in these regions as compared with the seismically more active southern Europe, there are very few joint analyses of earthquakes based on both instrumental and tectonic observations in the northwestern Alps. The main purpose of this paper is to present such a joint analysis focused on the largest instrumentally known earthquake in the French northern Alps, the Chamonix 1905 April 29 earthquake (Fig. 1). Its published moment magnitude M_w ranges between 5.1 and 5.6 (Bernardi et al. 2005, Alasset 2005, Cara et al. 2008, Fäh et al. 2011, and Rovida et al. 2011).

The largest instrumentally known earthquake in the nearby Valais canton occurred near Sierre on January 25, 1946, 60 km northeast of Chamonix (Fig. 1). Its magnitude ranges between Mw=5.8 (Bernardi et al. 2005) and M_w=6.1 (Fritsche & Fäh 2009). More recently, on July 15, 1996 a slightly damaging earthquake struck the city of Annecy, France, 60 km west of Chamonix (Thouvenot et al. 1998; M_w=4.7 (SI-Hex 2014)). Within a 30 km distance from Chamonix, two similar magnitude events are instrumentally recorded: an earthquake near Martigny on August 25, 1915 (M_w=4.6, Bernardi et al. 2005) and farther east near the border between the Valais canton in Switzerland and the Aosta county in Italy on September 23, 1938 (M_w=4.9, Rovida et al. 2011; M_w=4, Fäh et al. 2011). More recently, on September 8, 2005, at proximity to the SisFrance (2016) macroseismic epicentre of the April 29 1905 Chamonix earthquake, another earthquake occurred on September 8 2005 near the locality of Vallorcine, France (E3 in Fig. 3) with M_w= 4.5 ± 0.1 (Fréchet et al. 2011; M_w= 4.4 ± 0.1, Rovida et al. 2011; M_w= 4.7 ± 0.2, SI-Hex 2014). The microseismic activity of the area is shown in Figure 2 that displays instrumental data for the period 1984-2008 (ECOS-09; Fäh et al. 2011); note the alignment of micro-earthquakes along the Rhône valley – Salvan Fault zone (RVSF).

The recent 2005 Vallorcine earthquake located at the SW end of the RVSF line drawn in figure 2 revealed a right-lateral motion along a sub-vertical fault striking N60°E (Fréchet et al. 2011). In 2001, a swarm of small earthquakes ($M_w \leq 3.6$) occurred near the city of Martigny 15 km northeast of Vallorcine, close to the 1915 Martigny earthquake location. A set of fault segments striking ≈ N50°E was activated with a right lateral motion in 2001 (Deichmann et al. 2002). Delacou et al. (2005) propose that there is an « exclusively dextral transcurrent regime of deformation » within a series of faults striking parallel to the external crystalline massifs along a line “Wildhorn-Martigny”

(RVSF, in Fig.1). The 2005 Vallorcine earthquake fits well into this scheme. This interpretation may also be compatible with the general NW-SE directed compression scenario of the Mont Blanc and Aiguilles Rouges massifs advocated by Leloup et al. (2005) if we consider a transpressive regime. Dextral strike slip deformation within the Mont Blanc shear zone could still be active today (Egli & Mancktelow 2013). It could have been active, but in an overall thrust regime, either since 16 Ma until present following Rolland et al. (2007) or only between 12 and 4 Ma following Leloup et al. (2005; 2007).

Another tectonic regime could possibly be superimposed on this transpressive regime, namely normal faulting associated with erosion during the Alpine glaciation (Glotzbach et al. 2008, Vernant et al. 2013). The analysis of a large series of earthquake focal mechanisms in the western Alps shows an extensive stress regime within the inner Alps but not in the external domain where strike-slip events are dominant (Sue et al. 1999) while in a more detailed stress inversion, Delacou et al.(2004) found a NW-SE-directed extensional regime in the Chamonix area. Note that in a NW-SE compressive regime, local NW-SE extension along NE-SW striking normal faults is not incompatible when considering vertical crustal wedge extrusion (Brunel et al. 1994, Burchfiel et al. 1992).

In the present paper, we shed some light to the question of active tectonics in the Mont Blanc and Aiguilles Rouges massifs by further investigating details of the characteristics of the 1905 Chamonix earthquakes. Macroseismic, tectonic, and instrumental observations are confronted with several hypotheses on the origin of these 1905 earthquakes in sections 2, 3 and 4, respectively. Discussion of these observations in section 5 attempts to better document complex active tectonics of the region.

2. Macroseismic data

Maximum macroseismic effects of the April 29, 1905 Chamonix earthquake are observed in an area encompassing both the Mont Blanc and Aiguilles Rouges massifs (Fig. 3). The location of the macroseismic epicentre according to SisFrance (2016) is labelled E1 in Figure 3; the location after Guidoboni et al. (2007) is about 10km toward the SE (E1-bis in Fig. 3). Epicentral macroseismic intensity I_0 is between VII and VIII according to SisFrance (2016) on the MSK-64 scale (Sponheur & Karnik 1964). A second large earthquake occurred in the vicinity on August 13, 1905 (E2 in Figure 3). The magnitudes of both events determined from macroseismic data by Karnik (1969) are

very similar (M=5.7 and M=5.6, respectively), but they differ more in Rovida et al. (2011) (M=5.7 and M=5.1, respectively). The entire area in Figure 3 is referred to as the epicentral zone hereafter.

Original data show that the largest macroseismic effects of the April 29 earthquake are observed near Argentière north of Chamonix, (Christensen & Ziemendorff 1909, SisFrance 2016). Macroseismic intensity reaches IX on the Rossi-Forel scale (de Rossi 1883). Converted into modern intensity scales, this corresponds to VIII on both the MSK and EMS-98 scales (e.g. Levret et al. 1988, Cara et al. 2008). The August 13 maximum intensity is VI-VII in the Rossi-Forel scale (Christensen & Ziemendorff 1909). This corresponds to intensity VI MSK-64 according to Levret et al. (1988), and V-VI in both the MSK-64 and EMS-98 scales (Alasset 2005), and not to VII as postulated in SisFrance (2016). Furthermore, macroseismic epicentres of the April 29 (E1-bis) and August 13 events are very similar for Guidoboni et al. (2007). They are located 4km north of the August 13 SisFrance (2016) macroseismic epicentre (E2, Fig. 3). It is thus very likely that the August 13 earthquake is an aftershock, which occurred in proximity of the fault responsible for the April 29 main shock, somewhere on the upper part of the map shown in figure 3. In addition to the August 13 large aftershock, a series of at least ten small earthquakes are reported near Chamonix in SisFrance (2016), all likely to be aftershocks of the April 29, 1905 earthquake.

In order to answer the question of whether or not the same fault system is responsible for both the 1905 earthquakes (E1 or E1-bis and E2 in Fig. 3) and the 2005 Vallorcine earthquake (E3 in Fig. 3), instrumental data for the 1905 events are not accurate enough for locating the 1905 epicentres with precision. Indeed, among the 27 stations providing arrival time data for the April 1905 main shock, Szirtes (1909) reports 14 P-arrival times at distances between 134 km (Torino, Italy) and 874 km (Hamburg, Germany), but incoherency of several tenths of seconds among the reported first-arrival times makes locating the 1905 epicentres with sufficient accuracy hopeless. Detailed inspection of macroseismic observations is likely to provide us better information. For this reason, we re-examine and complement the macroseismic observations reported by Rothé (1941) and SisFrance (2016) hereafter. Because the August 13 1905 event (E2 in Fig. 3) occurred in summer, descriptions associated to its effects are much more numerous throughout the epicentral zone; we thus first describe the effects of the August 13 1905 event and then those of the April 29 1905 event (E1 or E1bis in Fig. 3), which occurred at night, just after heavy rain and snow falls.

The August 13 1905 earthquake occurred in the morning, when several persons were hiking in the Mont Blanc and Aiguilles Rouges massifs. On August 13, 1905, Lecarme (1906) made geodetic observations above the Col du Tour at 3280 m NE of Argentière (at location B2 in Figure 3). He

observed many rock-, ice- and snowfalls near the Glacier du Tour west and south of B2 (Figure 3). He furthermore reports an explosion-like noise heard in the proximity of Argentière. Among different rock-falls, which broadly affected the Mont Blanc and Aiguilles Rouges massifs, Lecarme (1906) concluded that the strongest effects of this earthquake are observed in the area around the Glacier du Tour where SisFrance (2016) located the epicentre (E2 in Fig. 3). Figure 3 also shows the places where the most significant effects were reported, and a brief summary of the effects is given in Table 1. Except for low frequency sounds preceding a strong ground shaking and rock-falls reported from the summit of Le Buet , 3096 m (de Quervin 1906), 3 km W of the 2005 Vallorcine epicentre E3 (B5 in Fig. 3), we found no other report from this NW sector of the study area (Table 1). The area near and around Argentière located within the upper Chamonix valley, is clearly where the reported effects are the strongest. The explosion heard in the immediate vicinity of Argentière (Table 1) further argues in favour of a very close location of the 1905 epicentre. In 2005, similar strong explosion-like noises were reported in the Vallorcine valley, in proximity of the epicentre E3 shown in Figure 3, while in the Chamonix valley further south most people reported a rumbling noise at that time (Cara et al. 2007).

In connection with the April 29 1905 main shock, damages to constructions are widely reported. The most serious damages occurred in Argentière (A6a in Fig. 3 and Table 1) and in its vicinity in Grassonet (A6b), La Joux (A5 and Fig. 4), and Les Tines (A6c). In Argentière most houses were heavily damaged with wide cracks in masonry walls. An unpublished note from an inhabitant reports that reinforcements with iron rods were necessary in many houses. These damages of grade 3 to 4 in many buildings of vulnerability class A are typical of intensity VII in the EMS-98 scale (Grünthal et al. 1998). To a lesser degree, cracks in houses and churches are also mentioned in Chamonix, Vallorcine (A9), Trient (A10), Martigny and, farther east in Grand-Saint-Bernard (Montandon 1942). Additional evidence for strong ground motion near Argentière are a landslide (A3 and Fig. 5) leading the railway company to change the course of the line (Le Roy 2008), deep cracks along the road between Argentière and Les Tines (**A7**), and an important 400 l/s flow of water gushing at the bottom of the landslide place (A2). The fall of a rock from the top of Aiguillette d'Argentière, just above Argentière (A1), is another observation reported by Charlet (1949) that wrote that this rock was present when his father climbed the top in 1885 for the first time. In Vallorcine, the church only presents "insignificant risk" as noted in the report of the town council of June 27, 1905. Farther to the NW, attempts to collect reports in the Samoëns valley, 10 to 15 km WNW of Vallorcine, were unsuccessful. Hence the shaking is likely to have caused only minor damages there, if any.

In summary, the location of the strongest macroseismic effects confirms that the April 29 and August 13 1905 epicentres are most likely located near Argentière in the upper part of the Chamonix valley as reported by Christensen & Ziemendorff (1909), and not in the Vallorcine valley located farther to the north. The fault system responsible for the two 1905 Chamonix earthquakes is thus likely different from that related to the recent 2005 Vallorcine earthquake.

3. Potential active faults in the Mont Blanc and Aiguilles Rouges massifs

Leloup et al. (2005) present a detailed structural sketch of the Mont Blanc and Aiguilles Rouges massifs (Fig. 6) together with a likely chronology of the activity of different fault zones. According to these authors, two fault zones could be presently active: the basal thrust fault dipping beneath the Aiguilles Rouges and Mont Blanc massifs, 5 to 15 km beneath sea level (Alpine sole thrust in Fig. 6), and a back thrust southeast of the Mont Blanc in the Courmayeur valley, Italy (Courmayeur Mont Blanc thrust, labelled CMBT in Fig.1). Activity of the steeply SE dipping Mont Blanc shear zone (Fig. 6) may have ended 4 Ma ago (Leloup et al. 2005, Glotzbach et al. 2008) although it may presently accommodate right-lateral shear (Egli and Mancktelow 2013). Not noticed as a possible active fault until the 2005 Vallorcine earthquake (E3 in Fig. 3) is a right-lateral strike slip fault, N of the Aiguilles Rouges massif, and SW of the Emosson lake, in continuity of the Rhône valley – Salvan fault zone (or Vallorcine – Valais shear zone, RVSF in Fig. 1) responsible for the small 2001 earthquake swarm (Deichmann et al. 2002), and possibly also responsible for the 1915 Martigny earthquake.

3.1 - The Vallorcine fault zone of the Vallorcine – Valais shear zone

The M_w=4.7 (±0.2) 2005 Vallorcine earthquake corresponds to a right-lateral rupture of a fault segment trending N60°E at 4 km depth below sea level (Fréchet et al. 2011; see epicentre F3 in Fig. 6). The rupture probably did not reach the surface during this earthquake but an apparently recent crack is visible in the 350 m-high gneiss block « Gros Nol » (Fig. 7) trending in the same azimuth as the elongated aftershock distribution and in agreement with the focal mechanism of the main shock (Fréchet et al. 2011). This trace of this fault could be the southwestern end of the right-lateral Wildhorn-Martigny fault zone of Delacou et al. (2005) that roughly corresponds to the Rhône Valley-Salvan shear zone (Figs. 1 & 6). This is a potential active fault segment if one considers the freshness of its trace prior to the 2005 event (Fig. 7).

3.2 - The Remuaz fault

The Remuaz fault (Fig. 6) corresponds to an ancient geological contact between the Aiguilles Rouges gneiss and the Vallorcine granite (Debelmas 1974, Ayrton et al. 1987), running for about 15 km between the Rhône and Chamonix valleys. At its southern end (Figs. 2, 8 and 9), the geomorphological characteristics of the fault are those of a slightly left-lateral normal fault trending N20, dipping 70° to the southeast, with very well marked steeply dipping striations oriented N85°E (Fig. 10; Alasset 2005). At a large scale, the Remuaz fault trace follows the structural direction of the Aiguilles Rouges massif and crosses the Col des Montets pass, a former glacial channel connected to the Rhône valley to the northeast. The fault is well marked in the landscape as a 40 to 60 m-high topographic step near the rim of the upper part of the glacial valley wall (Figs. 8 and 9) at an elevation below 2100 m a.s.l., thus below the highest glacial infill of the last glacial maximum (2400 m a.s.l. at the Last Glacial Maximum, LGM, 20 ka, Kelly et al. 2004; Fig. 9). The Remuaz fault separates two different types of rocks, granite in the Aiguilles Rouges in the footwall and gneiss in the hangingwall, thus the topographic step across the fault trace is either a result of differential glacial ablation during the LGM or it is the trace of an active fault which has been preserved despite several hundreds of meters of ice cover.

The upper part of the several tens of meters high scarp is degraded and convex upward, indicating long lasting erosion. Steeper parts in this upper part show clear sub-horizontal striations indicative of along strike glacial flow, in agreement with glacier channelling towards the Rhône valley as deduced from glacial striations compilations in the massif (Coutterand & Buoncristiani 2006). The basal part of the scarp shows very different aspects, in particular near its northern end above the Col des Montets pass (Figs. 8 and 9). There, the base of the scarp is a clean-cut steep wall with traces of steeply dipping striations that become a very clear going downwards the scarp. In addition, while most of the scarp is dark grey coloured and covered by lichens, the lower part of this scarp has been refreshed recently as it shows a light-coloured 20 cm-wide strip for a length of about 40 m, indicating that may have been recently exhumed. This probably freshly exhumed part of the scarp may be due to down-sliding or settling of the colluvial debris wedge in a very steep part of the valley wall, or it may be due to recent normal faulting slip, similar to commonly observed refreshed scarps after large earthquakes along normal fault scarps in Greece or Italy (e.g. Benedetti et al. 2003). In our case, no other recent event except for the 1905 event would be sufficiently large to produce shaking leading to slope destabilization or direct slip on the fault plane. We do not know how long it takes for freshly exposed rocks to regain their dark grey hue and the necessary climatic conditions are for lichens to grow and extend spatially. It thus remains speculative as to whether the observed exhumed basal scarp dates back to faulting or shaking in 1905, or if it is more recent and not of seismic origin.

247

248 3.3 - Cosmogenic ^{10}Be surface dating of glacial geomorphology

249 To better constrain the age of the geomorphological features near the Remuaz fault plane we
250 carried out cosmogenic ^{10}Be dating of glacially polished bedrock surfaces. While the maximum
251 infill of the LGM glaciers is about 300 m above our sampling site at ~2050 m a.s.l., this yields
252 a maximum age of 20 ka BP (Chapron 1999, Jorda et al. 2000) for the glacial morphology. The
253 timing of the different retreat stages (Coutterand & Nicoud 2005) is less well constrained,
254 mostly because the ages were determined in lake deposits near the front of the maximum
255 advances and because the reconstructions of the shape of the glacial volumes rest on few
256 moraine remnants. Clear frontal moranic ridges shown in Figure 9 straddle the southeastern
257 flank of the Aiguilles Rouges massif but they are likely due to the ending phases of the LGM
258 glacial period and not to the recent Little Ice Age.
259
260 We sampled two sets of samples (Table 4). REM1 originates from the steep glacially striated
261 slope of the fault scarp (Fig. 11b), therefore reducing the shielding effect by snow
262 accumulation. REM3, 4 and 5 were sampled near the base of the fault scarp, on glacially
263 striated rocks ("roche moutonnée"), usually covered by snow during the winter season (Fig.
264 11a).
265
266 As expected, Rem1 has a larger ^{10}Be concentration than the other samples, thus it is likely
267 slightly older than the three others, and we interpret this age of 15 ka as the time when glaciers
268 flowing from the Aiguilles Rouges massif stopped covering this part of the fault scarp. The
269 other samples are younger, 8-11 ka, despite their higher elevation (a few tens of meters),
270 probably because a snow correction is needed (Schildgen et al. 2005). Simple calculations
271 based on present day snow coverages may imply a 25 % correction for the 8-11 ka ages, i.e. 2-3
272 ka (e.g. Gosse & Phillips 2001, Mériaux et al. 2009). The precision of this correction is highly
273 dependent on the knowledge of past snow or ice coverages at a local level, which are not
274 known.
275
276 In summary, the ages obtained indicate an early retreat of the glaciers (~15 ka) right after the
277 LGM as suggested by Coutterand & Nicoud (2005). If the basal 5 meters of the scarp were
278 exhumed seismically after glacial retreat as suggested by georadar profiles made at the bottom
279 of the fault (Alasset 2005), then this timing provides an upper bound of tectonic movement and
280 a possible average rate of about 0.3 mm/yr. Given the 70° dip of the fault and the assumed
281 simplified structural geometry of Figure 6 suggesting upward extrusion of an Aiguilles Rouges
282 crustal wedge, this rate may correspond to less than 1 mm/yr perpendicular shortening on the
283 basal thrust and locally surface extension at the location of the Remuaz fault (Fig. 6).
284

4. Instrumental data and waveform modelling

4.1- Seismic waveform records

Among the different seismic stations running in 1905, very few were equipped with well-calibrated, damped instruments. Furthermore, modelling the full seismic waveform at regional distances requires computation of Green's functions adapted to the 3D regional structure between the epicentre and the seismic stations. This is out of the scope of the present study limited to long-period surface waves that smooth out the structures due to their large wavelengths.

In 1905, the number of seismic stations eligible for such modelling is small. The best-suited instrument for this approach is the 1-ton Wiechert inverted pendulum. The records of Göttingen (Germany) and Uppsala (Sweden) are shown in Figures 12, 13 and 14. The instrumental parameters of the corresponding 1905 seismographs are given in Table 2.

4.2 Magnitudes of the April 29 and August 13, 1905 earthquakes

Surface-wave magnitudes M_S of the main shock determined from the records shown in Figures 12 and 13 are given in Table 2 according to the IASPEI formula (Vanek et al. 1962):

$M_s = \log_{10}(A/T)+1.66\log_{10}(D) + 3.3$,

where A is the maximum amplitude of the ground motion at period T, and D is the epicentral distance in degree. Depending on the station and component considered, M_s covers the range [4.9, 5.5] with an averaged value M_s=5.1.

In Göttingen, where the August 13 event is well recorded (Fig. 14), the ratio between maximum amplitudes of the April 29 and August 13 events taken from the East component where the signal is the largest yields a difference of M_s close to unity. The surface-wave magnitude of the August 13 aftershock can thus be set between 3.9 and 4.5, depending on the magnitude of the April 29 event. It is thus much smaller than those reported in the literature so far (Karnik 1969, Rovida et al. 2011). This difference of magnitudes of around 1 reinforces the conclusion drawn in section 2 that the August 13 event is very likely an aftershock of the April 29 event according to the Bath's law (Båth 1965).

4.3 Waveform modelling

In order to test how different focal mechanisms are compatible with the recorded waveforms, synthetic seismograms are computed for the Göttingen and Uppsala records. Computations are

performed with version 3.30 of the code of Hermann (2013) and a Green's function corresponding to the CRUST2.0 model (Bassin et al. 2000) averaged along the paths between the SisFrance (2016) April 29, 1905 epicentre and the seismic stations. Fitting the raw Wiechert records is not possible with such a 1-D Green's function because of a too simple representation of the elastic structure between the epicentres and the stations. In turn when applying a low-pass filter to both the records and the synthetics, satisfactory fits are obtained. In the application presented here we apply a Butterworth band-pass filter with corner frequencies at 0.02 Hz and 0.07 Hz with two poles and two zeros.

Criteria for testing the quality of the fit are the overall correlation coefficient r and a misfit function m computed over the combined lengths of the records at the two stations:

$$r = \frac{\sum_{i,n} w_n \left({}^{n}O_i \, {}^{n}S_i \right)}{\sqrt{\sum_{i,n} w_n \, {}^{n}O_i^2} \sqrt{\sum_{i,n} w_n \, {}^{n}S_i^2}}, \text{ and } , \quad m = \frac{\sum_{i,n} w_n \left| {}^{n}O_i - {}^{n}S_i \right|}{\sum_{i,n} w_n \left| {}^{n}O_i \right|}$$

where ${}^{n}O_i$ is the zero-mean observed seismogram at station-component n and time sample i , ${}^{n}S_i$ is the corresponding zero-mean synthetic seismogram, and w_n is the weight applied to the data n. The misfit function m varies from 1 for a null synthetic signal to zero when the fit is perfect, and it grows as the seismic moment at large magnitudes. Here, the weights w_n are set to 1 in Göttingen, and 0.3 (East component) and 0.1 (North component) in Uppsala in order to take into account the signal-to-noise ratio estimated by visual inspection of the seismograms shown in Figures 12 and 13. Finally, because of the large uncertainty in the origin time of the earthquake and in order to take into account uncertainty in group arrival times, a time-shift correction is applied at each station in order to maximize the correlation coefficient r.

Five focal mechanisms F1 to F5 and, for each mechanism, three depths h (5, 10 and 15 km) are tested in the computations (Table 3, Fig. 16). Focal mechanism F1 is a good overall compromise between maximum correlation r and minimum misfit m. Focal mechanism F1 is found without any a priori geological information by applying a coarse grid-search technique in the parameter space (strike ϕ, dip δ, rake λ, and crustal depths h) with a fixed half duration $\tau/2$=1s. Focal mechanism F2 corresponds to the strike, dip, and rake of the Remuaz fault as observed in the field (Figs. 9 and 10). The F2 synthetic seismograms shown in Figure 15 fit the records with a better correlation than F1 for a source at 5 km depth, although with a slightly smaller correlation and larger misfit for deeper source (Table 3). Focal mechanism F3 corresponds to the right-lateral strike-slip mechanism of the 2005 Vallorcine earthquake (Global CMT 2014). Correlation r *is* lower than 0.4 and misfit m is larger than unity for this F3 mechanism (Table 3). This is the worst fit among the tested solutions.

F4 corresponds to a thrust fault mechanism within the Mont Blanc Shear Zone and F5 is a hypothetical focal mechanism corresponding to the basal thrust beneath the Aiguilles Rouge massif (Fig. 6). Both mechanisms F4 and F5 present rather good correlation coefficients *r*, larger than 0.7 for *h*=5 km, but a large misfit *m* above 0.8 whatever the depth choice. These mechanisms thus cannot be completely excluded but are less likely than F1 and F2. Note that F1 is a pure sinistral strike-slip mechanism not supported by geological observation.

In Table 3, M_w is adjusted in order to independently minimize the misfit at Göttingen and Uppsala, while in Figure 16 a common value of M_w is used in the computation for both stations. This figure shows how the misfit function *m* varies with M_w for the different focal mechanisms and a fixed depth *h*=5 km. It confirms that the smallest misfits are obtained for mechanisms F1 (M_w=5.1) and F2 (M_w=5.3). Table 3 and Figure 16 show that extreme values of M_w obtained vary between 5.0 and 5.5 with an averaged value of 5.3 and a preferred value of 5.3 if one selects the focal mechanism corresponding to the Remuaz fault (F2).

In conclusion, this waveform experiment is not very conclusive to discriminate between the possible focal mechanisms. However, it favours the Remuaz fault as the most likely source fault of the 1905 earthquake and it shows that the right lateral fault mechanism of the 2005 Vallorcine earthquake presents the worst fit amongst the observed 1905 seismograms.

5. Discussion

Structural geology and tectonic geomorphology show that at least 2 fault systems have clear surface expressions that may result from repeated earthquakes or large surface rupturing events. The 2005 Mw=4.7 Vallorcine earthquake, while clearly not a surface rupturing event, nevertheless occurred down-dip from clear surface bedrock cracks with similar kinematics that may indicate a genetic link (Fréchet et al. 2011). While cracks may be preserved for long time in bedrock outcrops, the Gros Nol surface cracks have an apparent freshness that seems to indicate recent movement. From the observations made at present it is not possible to determine the minimum magnitude of earthquake events responsible of these cracks. However, because they are located at the southwestern end of the ~ 50 km-long fault zone mentioned by Delacou et al. (2005), it is not unlikely that a larger magnitude earthquake could also occur there.

The other fault system with a clear surface expression within the epicentral zone of the 1905 Chamonix earthquakes is the Remuaz fault. Its kinematics is clear. It shows up clearly in the landscape as a decametric scarp for several kilometres and has thus to be explained in view of the late glacial occupation of the Chamonix and Vallorcine valleys during the LGM and after (15 ka). What is more ambiguous is whether the exhumation of the lower striated part of the scarp and the more recent white strip at its base are due to seismic activity. Indeed, this part of the fault or scarp is also where the valley slope is the steepest and slope instability above the Col des Montets pass cannot be excluded. If an event of M_w=5.3 is responsible for the 20 cm-high and 40 m-long exhumed base of the scarp then it must have occurred in the first five kilometres of the crust. Another possibility remains, that even without primary surface slip, slope instability may be triggered by shaking due to nearby or deeper earthquakes.

In order to discriminate between the Vallorcine fault zone as part of the Vallorcine – Valais shear zone and the Remuaz fault, macroseismic analysis of original reports coming from the epicentral zone provides arguments to favour the hypothesis that the main shock is not located near the epicentre of the 2005 Vallorcine earthquake and thus that the 2005 and 1905 earthquakes did not occur along the same structure. Although both structures are distant by only 5 km, macroseismic observations would rather place the main shock and its larger aftershock near Argentière in the upper part of the Chamonix valley, NE of the southern termination of the surface trace of the Remuaz fault.

An additional argument may be drawn from the waveform modelling of the Göttingen and Uppsala Wiechert records. Although not very conclusive for the focal mechanisms tested and although sensitivity of the seismogram fits to depth of the focus is very loose, the modelling favours the quasi-normal motion on the Remuaz fault as compared to the right-lateral motion on the Vallorcine fault system. Waveform fit and correlation to the observed seismic waveforms is less good for the thrust motions within the Mont Blanc shear zone and beneath the Aiguilles Rouges but these focal mechanisms cannot be excluded provided the hypocentre is rather shallow (mechanisms F4 and F5 in Table 3. Note that a rather shallow hypocentre is also supported by macroseismic observations. The pattern of macroscopic effects concentrated in a radius of about 5 km is not compatible with a focus at 15-20 km depth at the bottom of the seismogenic zone within the plunging lithosphere because it would spread maximum macroseismic effects over a much broader zone. Independently, the explosion-like noise clearly reported after the August 13 aftershock is in favour of a rather surficial hypocentre, similar to that of the 2005 Vallorcine earthquake.

Extension perpendicular to the trend of the Aiguilles Rouges massif such as that associated with the quasi-normal Remuaz fault is compatible with the extensional stress regime along the axial zone of the entire Western Alps, including the Chamonix area, deduced from the analysis of focal mechanisms by Delacou et al. (2004). Such extension is attributed either to gravitational flow following the end of tectonic shortening, and possibly as a consequence of anti-clockwise rotation of Apulia (Delacou et al. 2004, Fréchet et al. 1996, 2011, Thouvenot et al. 2003, Champagnac et al. 2006), or to vertical tectonic movement due to slab break-off (Baran et al. 2014) leading to high rates of exhumation coupled with extension (Fox et al. 2016), or to global climatic change (Champagnac et al. 2009). However, parts of the extension-like deformation southeast of the Aiguilles Rouges massif could also be related to the upward extrusion of an Aiguilles Rouges crustal wedge in a shortening context (e.g. Leloup et al. 2005, Masson et al. 2002, Malavieille, 2010) as suggested from the simplified structural cross section (Fig. 6). Possibly, tectonic stresses acting in a region of slow strain rates together with post glacial isostatic adjustments to rapidly eroding mountain ranges, could explain why such different fault systems as the Vallorcine and Remuaz faults may be active over only a few kilometres distance.

6. Conclusion

This combined study sheds new light on a moderate size earthquake of the Alps. It contributes towards locating it at close proximity of Agentière in the upper part of the Chamonix valley and to firmly determine the second shock of August 13 1905 as an aftershock of the April 29 1905 as the main shock. Waveform modelling of seismograms recorded in Göttingen and Uppsala yields a magnitude Mw=5.3 (±0.3) for the April 29 main shock, while inspection of the records of the August 13 event in Göttingen argues in favour of a magnitude about one unit smaller.

Source depth and focal mechanism of the April 29 main shock remain poorly determined from instrumental data. Among the tested mechanisms, forward modelling of the few waveforms available, based on a priori fault models, favours a N20 striking quasi normal fault corresponding to the strike of the Remuaz fault, and a poorly determined depth of 5 km. However, two thrust mechanisms, a shallow angle thrust beneath the Aiguilles Rouges massif and a thrust fault within the broad Mont Blanc Shear Zone cannot be excluded. In turn, an event with a dextral strike-slip focal mechanism similar to the 2005 Vallorcine earthquake can probably be excluded.

While the geomorphological expression and kinematic indicators of the Remuaz fault scarp could correspond to the surface trace of the fault that broke in 1905, the N20 along-strike observations located along the steepest valley walls may also be related to slope instability. Surface exposure dating in the hangingwall at the base of the decametric scarp indicates glacial retreat after 15 ka and concurs for post-glacial normal faulting. Whether our observations correspond to present-day seismotectonic activity or to a gravitational cause remains to be determined in the future.

Aknowledgements

We thank M. Meghraoui, J. Fréchet, and S. Coutterand for insightful discussions and data sharing. Daniel Egli and an anonymous referee help us greatly improve a former version of the manuscript. D. Ancey is thanked for communicating the Gros Nol photo of 1973 by B. Leclerc, and J. Ravanel for communicating a report by an anonymous Argentière inhabitant. MC thanks L. Rivera for advices during the waveform modelling computations, and O. Kulhanec in Uppsala and the former staff of Göttingen observatory for information on instrumental parameters.

References

Alasset, P.J. (2005). Sismotectonique et identification des sources sismiques en domaine de déformation lente : cas des Pyrénées Occidentales et des Alpes du Nord (France). Le Tsunami créé par le séisme de Zemmouri (Mw=6.9, Algerie) du 21 mai 2003. *Ph.D. thesis*, University of Strasbourg, 214 pp.

Armijo, R., Deschamps A., Poirier, J.P. (1986). *Carte sismotectonique – Europe et Bassin méditerranéen*, Institut de physique du globe, Paris.

Ayrton, S., Barféty, J.C., Bellière, J., Gubler, Y., Jemelin L. (1987). *Carte géologique de Chamonix (1/50000)*. BRGM. Orléans.

Balco, G., Stone, J.O., Lifton, N.A., Dunaï, T.J. (2008). A complete and easily accessible means of calculating surface exposure ages or erosion rates from ^{10}Be and ^{26}Al measurements. *Quaternary Geochronology*, *3*, 174-195.

Baran, R., Friedrich, A.M., Schlunegger, F. (2014). The late Miocene to Holocene erosion pattern of the Alpine foreland basin reflects Eurasian slab unloading beneath the western Alps rather than global climate change. *Lithosphere, 6/2*, , 124-131.

Bassin, C., Laske, G., Masters, G. (2000). The Current Limits of Resolution for Surface Wave Tomography in North America. *EOS Transactions AGU*, *81*, F897.

Båth, M. (1965). Lateral inhomogeneities in the upper mantle. *Tectonophysics, 2*, 483-514.

Benedetti, L. Finkel, R., King, G., Armijo, R., Papanastassiou, D., Ryerson, F.J., Flerit, F., Farber, D., Stavrakis G. (2003). Motion on the Karapelli fault (Greece) prior to the 1981 earthquake sequence determined from 36Cl cosmogenic dating. *Terra Nova, 15*, 118-124.

Bernardi, F., Braunmiller, J., Giardini, D. (2005). Seismic Moment from Regional Surface-Wave Amplitudes: Applications to Digital and Analog Seismograms. *Bulletin of the seismological Society of America*, *95*, 408-418.

Brunel, M., Arnaud N., Tapponnier, P., Pan, Y., Wang, Y. (1994). Kongur Shan normal fault: type example of mountain building assisted by extension (Karakoram fault, eastern Pamir). *Geology*, *22*, 707-710.

Burchfiel, B.C., Chen, Z., Kip, V.H., Liu, Y., Leigh, H.R., Deng, C., Xu, J. (1992). The South Tibetan Detachment system, Himalayan Orogen: extension contemporaneous with and parallel to shortening in a collisional mountain belt. *Geological Society of America Special Paper 269*, 1-46.

Cara, M., Schlupp, A., Sira, C. (2007). *Observations sismologiques: sismicité de la France en 2003, 2004, 2005* (199 pp.). Bureau Central Sismologique Français, ULP/EOST-CNRS/INSU, Strasbourg.

Cara, M., Alasset, P.J., Sira, C. (2008). Magnitude of historical earthquakes, from macroseismic data to seismic waveform modelling: application to the Pyrenees and a 1905 earthquake in the Alps. In J. Fréchet, M. Meghraoui & M. Stucchi (Eds.). *Historical Seismology Interdisciplinary Studies of Past and Recent Earthquakes Serie*, *Modern Approaches in Solid Earth Sciences*, *2*, (pp. 363-378). Springer.

Champagnac, J.-D., Sue, C., Delacou, B., Tricart, P., Allanic, C., Burkhard, M. (2006). Miocene lateral extrusion in the inner western Alps revealed by dynamic fault analysis. *Tectonics 25/3*. Doi:10.1029/2004tc001779.

510 Champagnac, J.D., Schunegger, F., Norton, K., Von Blanckenburg, F., Abbühl, L. M., Schwab, M. (2009).
511 Erosion-driven uplift of the modern Central Alps. *Tectonophysics*, *474*, 236-249, doi:
512 10.1016/j.tecto.2009.02.024.
513 Chapron E. (1999). Contrôles climatiques et sismo-tectoniques de la sedimentation lacustre dans l'avant-
514 pays alpin (lac du Bourget) durant le Quaternaire recent. *Géologie Alpine*, *Mémoire H.S.*, *30*, p. 261.
515 Charlet, A. (1949). *Vocation alpine* (206 pp.). *Editions Victor Attinger*, Neuchatel, Paris.
516 Charlier, C. & Van Gils, J.M. (1953). *Liste des stations sismologiques mondiales* (282 pp.). Observatoire
517 Royal de Belgique, Uccle.
518 Christensen A. & Ziemendorff, G. (1909). *Les tremblements de terre ressentis pendant l'année 1905* (543
519 pp.). Bureau Central de l'Association Internationale de Sismologie, série B. Catalogue – partie I,
520 Strasbourg.
521 Coutterand, S. & G. Nicoud (2005). Les stades de retrait du glacier de l'Arve entre le verrou de Cluses et
522 l'ombilic de Chamonix au cours du Tardiglaciaire (Vallée de l'Arve, Haute-Savoie). *Quaternaire*, *16*,
523 85-94.
524 Coutterand, S. & Buoncritiani, J.F. (2006). Paléogéographie du dernier maximum glaciaire du pléistocène
525 récent de la région du massif du Mont Blanc, France. *Quaternaire*, *17*, 35-43.
526 Cuenot, S. (2015). *Le roman de Chamonix* (401 pp.). Editions Guérin, Chamonix.
527 Debelmas, J. (1974). *Géologie de la France, Les Chaînes plissées du cycle Alpin et leur avant-pays Vol II*
528 (544 pp.). Editions Doin. Paris.
529 Deichmann, N., Baer, M., Braunmiller, J., Ballarin Dolphin, D., Bay, F., Bernardi, F.,elouis, B., Fäh, D.,
530 Gerstenberger, M., Giardini, D., Huber, S., Kradolfer, U., Maraini, S., Oprsal, I., Schibler, R., Schler,
531 T., Sellami, S., Steimen, S., Wiemer, S., Wössner, J., Wyss, A. (2002). Earthquakes in Switzerland and
532 surrounding regions during 2001. *Eclogae geologicae Helvvetiae*, *95*, 249-261.
533 Delacou, B., Sue, C., Champagnac, J.D., Burkhard, M. (2004). Present day geodynamics in the bend of the
534 western and central Alps as constrained by earthquake analysis. *Geophysical Journal International*,
535 *158*, 753–774.
536 Delacou, B., Deichmann, N., Sue, C., Thouvenot, F., Champagnac, J.D., Burkhard, M. (2005). Active strike-
537 slip faulting in the Chablais area (NW Alps) from earthquake focal mechanisms and relative locations.
538 *Eclogae geologicae Helv*etiae *98*, 189–199.
539 Egli D. & Mancktelow N. (2013). The structural history of the Mont Blanc with regard to models for its
540 recent exhumation. Swiss Journal of Geosciences, 106, 469–489, doi : 10.1007/s00015-013-0153-5.
541 Fäh, D., Giardini, D., Kästli, P., Deichmann, N., Gisler, M., Schwarz-Zanetti, G., Alvarez-Rubio, S., Sellami,
542 S., Edwards, B., Allmann, B., Bethmann, F., Wössner, J., Gassner-Stamm, G., Fritsche, S., Eberhard,
543 D. (2011). *ECOS-09 Earthquake Catalogue of Switzerland Release 2011. Report and Database. Public*
544 *catalogue, 17.4.2011*. Swiss Seismological Service ETH Zürich, Report SED/RISK/R/001/20110417.
545 Fäh, D., Moore, J.R., Burjanek, J., Iosifescu, I., Dalguer, L., Dupray, F., Michel, C., Woessner, J., Villiger,
546 A., Laue, J., Marschall, I., Gischig, V., Loew, S., Marin, A., Gassner, G., Alvarez S., Balderer, W.,
547 Kästli, P., Giardini, D., Iosifescu, C., Hurni, L., Lestuzzi, P., Karbassi, A., Baumann, C., Geiger, A.,

548 Ferrari, A., Laloui, L., Clinton, J., Deichmann, N. (2012). Coupled seismogenic geohazards in Alpine
549 regions. *Bolletino di Geofisica Teoretica e Applicata, 53*, 485-508.
550 Fox, M., Herman, F., Willet, S.D., Schmid, S. (2016). The exhumation history of the European Alps
551 inferred from linear inversion of thermometric data. *American Journal of Science, 316*, 505-541.
552 Fréchet, J., Thouvenot, F., Jenatton, L. Hoang-Trong, Pho, Frogneux, M. (1996). Le séisme du Grand-
553 Bornand (Haute-Savoie) du 14 décembre 1994: un coulissage dextre dans le socle subalpin. *Comptes*
554 *Rendus de l' Académie des Sciences Paris, 323*, 517-524.
555 Fréchet, J., Thouvenot, F., Frogneux, M., Deichmann, N., Cara, M. (2011). The Mw 4.5 Vallorcine (French
556 Alps) earthquake of 8 september 2005 and its complex aftershock sequence. *Journal of Seismology,*
557 *15*, 43-58.
558 Fritsche, S. & Fäh, D. (2009). The 1946 magnitude 6.1 in the Valais: site-effects as contributor to the
559 damage. *Swiss Journal of Geoscences*, *102*, 423-439.
560 Gide, J.P. & Banaudo, A. (1998). *Les trains du Mt Blanc, Vol. 1* (195 pp.). Ed. du Capri.
561 Global CMT (2014). Global CMT catalog date: 2005/09/08, Chamonix event id: 200509081127A
562 http://goo.gl/PVg3Py (last access November 2014).
563 Glotzbach, C., Reinecker, J., Daniski, M., Rahn, M., Frisch, W., Spiegel, C. (2008). Neogene exhumation
564 history of the Mont Blanc massif, western Alps. *Tectonics*, *27*, TC4011, doi:10.1029/2008TC002257.
565 Gosse, J.C. & Phillips, F.M. (2001). Terrestrial in situ cosmogenic nuclides: theory and application.
566 *Quaternary Science Reviews*, *20*, 1475-1560.
567 Grünthal, G., Musson, R.M.W., Schwarz, J., Stucchi, M. (eds.) (1998). *European Macroseismic Scale 1998*
568 *EMS-98*, *Cahiers du Centre Européen de Géodynamique et de Séismologie, 15* (99 pp.), Luxembourg.
569 Guidoboni, E., Ferrari, G., Mariotti, D., Comastri, A., Tarabusi, G., Valensise, G. (2007). CFTI4Med,
570 Catalogue of Strong Earthquakes in Italy (461 B.C.-1997) and Mediterranean Area (760 B.C.-1500).
571 INGV-SGA. http://storing.ingv.it/cfti4med, accessed May 25, 2016.
572 Hermann, R. (2013). Computer programs in seismology: An evolving tool for instruction and research.
573 *Seismological Research Letters*., *84*, 1081-1088, doi:10.1785/022011009.
574 Jorda, M., Rosique, T., Evin, J. (2000). Données nouvelles sur l'âge du dernier maximum glaciaire dans les
575 Alpes méridionales françaises. *Comptes Rendus de l' Académie des Sciences Paris 331*, 187-193.
576 Karnik, V. (1969). *Seismicity of the European Area, Part 1* (364 pp.). *Reidel*, Dordrecht.
577 Kelly, M.A., J.-F. Buonchristiani, J.F., Schlüchter, C., (2004). A reconstruction of the last glacial maximum
578 (LGM) ice-surface geometry in the western Swiss Alps and contiguous Alpine regions in Italy and
579 France. *Eclogae Geologicae Heletiae*, *97*, 57-75.
580 Lal, D. (1991), Cosmic ray labeling of erosion surfaces: in situ nuclide production rates and erosion models.
581 *Earth and Planetary Science Letters*, *104*, 424-439.
582 Lecarme, J. (1906). Le tremblement de terre du 13 août observé en haute montagne. *La montagne, Club*
583 *Alpin Français*, *9*, 421-425.

584 Leloup, P.H., Arnaud, N., Sobel, E.R., Lacassin, R. (2005). Alpine thermal and structural evolution of the
585 highest external crystalline massif : the Mont Blanc. *Tectonics*, *24*, TC4002,
586 doi:10.1029/2004TC001676.
587 Leloup, P.H., Arnaud, N., Lacassin, R., Sobel, E.R. (2007). Reply to comment by Y. Rolland et al. on
588 ''Alpine thermal and structural evolution of the highest external crystalline massif: The Mont Blanc''.
589 *Tectonics*, *26*, TC2016, doi:10.1029/ 2006TC002022.
590 Le Roy, P.L. (2008). *Le Mont-Blanc Express* (158 pp.). Ed. Glénat, Grenoble.
591 Levret, A., Loup, C., Goula, X. (1988). The Provence earthquake of 11th June 1909 (France). A new
592 assessment of near field effects. In Seismic hazard in Mediterranean regions. In J. Bonnin; M. Cara, A.
593 Cisternas, R. Fantechi (Ed.), *Modern Approaches in Geophysics*, (pp. 383-399). Kluwer Academic
594 Publishers, Dordrecht.
595 Malavieille, J. (2010). Impact of erosion, sedimentation and structural heritage on the structure and
596 kinematics of orogenic wedges : analog models and case studies. *Geological Society of America, GSA*
597 *Today, 20/1*, doi: 10.1130/GSATG48A.1.
598 Masson, F., F. Gal, Leloup, P.H. (2002). Une carte gravimétrique hature rsolution du massif du Mont-Blanc:
599 implications structurales. *Comptes Rendus Geoscience, 334*, 1011-1019.
600 Meriaux, A.-S., K. Sieh, R. C. Finkel, C. M. Rubin, M. H. Taylor, A. J. Meltzner, Ryerson, F.J. (2009).
601 Kinematic behavior of southern Alaska constrained by westward decreasing postglacial slip rates on the
602 Denali Fault, Alaska, *Journal of Geophysical Research*, *114*, B03404, doi:10.1029/2007JB005053.
603 Montandon, F. (1942). Les séismes de forte intensité en Suisse. *Revue pour l'étude des calamités*, *5*, 167-
604 168.
605 Nishiizumi, K., Imamura, M., Caffee, M. W., Southon, J. R., Finkel, R. C., McAninch, J. (2007), Absolute
606 calibration of 10 Be AMS standards. *Nuclear Instruments and Methods in Physics Research Section B:*
607 *Beam Interactions with Materials and Atoms*, 258, 403-413, doi:10.1016/j.nimb.2007.01.297.
608 Plan-séisme (2015). Zonage sismique de la France. http://www.planseisme.fr/Zonage-sismique-de-la-
609 France.html, accessed May 25, 2016.
610 Quervin (de), A. (1906). Die Erdbeben der Schweiz im Jahre 1905. *Annalen der schweizerischen*
611 *meteorologischen Centralanstalt, year 42*, p.8.
612 Rolland, Y., Corsini, M., Rossi, M., Cox, S.F., Pennacchioni, G., Mancktelow, N., Boullier, A.M. (2007).
613 Comment on « Alpine thermal and structural evolution of the highest external crystalline massif: the
614 Mont Blanc » by P.H. Leloup, N. Arnaud, E.R. Sobel, and R. Lacassin. *Tectonics*, *26*, TC2015, doi :
615 10.1029/2006TC001956.
616 Rossi (de), M.S. (1883). Programma dell'osservatorio ed archivio centrale geodinamico. *Bullettino del*
617 *Vulcanismo Italiano*, *Anno X*, *n°3-5*, 49-128.
618 Rothé, J.P. (1941). Les séismes des Alpes françaises en 1938 et la séismicité des Alpes occidentales. In E.
619 Rothé (Ed.), *Annales de l'Institut de Physique du Globe, T3,* 52-53, Strasbourg.
620 Rovida A, Camassi R, Gasperini P, Stucchi M (2011). *CPTI11, the 2011 version of the Parametric*
621 *Catalogue of Italian Earthquakes*. http://emidius.mi.ingv.it/CPTI, accessed June 15, 2016.

622 SI-Hex (2014). *Sismicité de la France métropolitaine sur la période 1962-2009*.
623 http://www.franceseisme.fr/sismicite.html, accessed May 25, 2016.
624 SisFrance (2016). *Sismicité historique de la France- Métropole*, http://www.sisfrance.net/donnees_dates.asp,
625 accessed may 25, 2016.
626 Schildgen, T.F., Phillips, W.M., Purves, R.S. (2005). Simulation of snow shielding corrections for
627 cosmogenic nuclide surface exposure studies. *Geomorphology, 64*, 67-85.
628 Sponheuer, W. & Karnik, V. (1964). *Neue seismiche Skala*. In W. Sponheuer (Ed.), Proceedings 7th
629 Symposium of the ESC, Jena 24-30 Sept. 1962 (pp. 69-76). Veröffentlichungen Zentralinstitut für
630 Bodendynamik und Erdbebenforschung Jena der Deutschen Akademie der Wissenschaften, 7.
631 Stone, J. O. (2000). Air pressure and cosmogenic isotopes production, *Jornal of Geophysical Research*,
632 *105(B10)*, 23753-23759.
633 Sue C., Thouvenot F., Fréchet J. (1999). Widespread extension in the core of the western Alps revealed by
634 earthquake analysis. *Journal of Geophysical Research, 104 (B11)*, 25611-25622.
635 Szirtes, S. (1909). Katalog der im Jahre 1905 registrierten seismischen Störungen. *Publications du Bureau*
636 *Central de l'Association Internationale de Sismologie, Série B Catalogue partie II,* p.18, Strasbourg.
637 Thouvenot, F., Fréchet, J., Tapponnier, P., Thomas, J.-C., Le Brun, B., Menard, G., Lacassin, R., Jenatton,
638 L., Grasso, J.-R., Coutant, O., Paul, A., Hatzfeld, D. (1998). The Ml 5.3 Epagny (French Alps)
639 earthquake of 1996 July 15: a long-awaited event on the Vuache Fault. *Geophysical Journal*
640 *International, 135*, 876-892.
641 Thouvenot, F., Fréchet, J., Jenatton L., Gamond, J.-F. (2003). The Belledone Border Fault: identification of
642 an active seimic strike-slip fault in the western Alps. *Geophysical Journal International, 155*, 174-192.
643 Vallot, C. (1939). Massif du Mont-Blanc / Chamonix-Sixt. *Carte itinéraire à l'échelle de 1: 60 000,* Girard
644 et Barrère editions, Paris.
645 Vaneck, J., Zatopek, A., Karnik, V., Kondorskaya, N. V., Riznichenko, Y. V., Savarensky, E. F., Soloviev,
646 S. L., Shebalin, N.V. (1962). Standardization of magnitude scales. *Bulletin of the Academy of Sciences*
647 *of the USSR Geophysical Series* 108-111.
648 Vernant, P., Hivert, F., Chéry, J., Steer, P., Cattin, R., Rigo, A. (2013). Erosion-induced isostatic rebound
649 triggers extension in low convergent mountain ranges. *Geology, 41*, 467-470. doi:10.1130/G33942.1.
650

651

1-a Mainshock April 29, 1905, t_0 = 1h 47 min UT (this study), 1h 59 min (Sisfrance, 2016)		
Location	Effect	References
Argentière (B1)	• Main damages in Argentière : - Important cracks in most houses - *Church severely damaged* - *School to be repaired*	- Le messager agricole du Chablais May 6, 1905 - *Council meeting, June16, 1905.*
Aiguillette d'Argentière (A1)	• Fall of a rock overlooking the summit	- J. Ravanel (pers. com.) - Charlet (1949)
Near Argentière (A2)	• New spring	Revue savoisienne, T46,1905
Argentière - Le Planet (A3)	• Landslide	CAF n°5, 1906 Le Roy, 2005: fig. 2.3
Planet (A4)	• Hotel to be repaired	CAF n°5, 1906
La Joux (A5)	• Partial collapse of a house	S. Cuenot, 2015; Fig.2.2
Grassonet and Les Tines (A6)	• Slight damage in Grassonet and Les Tines schools	Council meeting, June16, 1905.
Road Argentière - Les Tines (A7)	• Deep cracks along and across the main road over a 800m-long section, likely located on an old glacier moraine	- Le cultivateur savoyard, n°18, May 4, 1905 - CAF I, 240, 1905 - De Quervin, (1906)
La Poya A8	• No damage in the newly built hotel	M. Chamel (pers. com.)
Vallorcine (A9)	Cracks in house walls, Cracks and plaster falls in the church *Insignificant damage in the church*	- Le messager agricole du Chablais May 6, 1905 - *Council meeting June 27, 2005*
Chamonix (fig.2.1)	• Many cracks in houses • People frightened	Cultivateur savoyard, n°18, May 4, 1905
Aoste, Italy	• Cracks in the ceiling • People frightened	Le Mont Blanc – Aoste, May 5, 1905
Trient (A10)	Wall collapse	Buhrer, Archives Sc. Phys. Et Nat., Genève 1905
Martigny (fig.1)	• Cracks in the church	Buhrer, Archives Sc. Phys. Et Nat., Genève 1905
Martigny (fig. 1)	• Church seriously damaged • Several chimney falls • Cracks in several houses	Montandon (1942)
Grand Saint-Bernard pass (fig. 1)	• Many damages	Montandon (1942)

652
653
654

1-b	**Aftershock** August 13, 1905, t_0 = 10h 22 min (this study and Sisfrance, 2016)		
*	Location	Effect	References
	B1 Argentière	• Strong blast heard • Partial collapse of the church vault • Displacement of the bridge pillars	Falconnet CAF, II, 425, 1906.
	B2 Col du Tour	• Strong shaking during 3-4 seconds • Rock and ice falls	Lecarme (1906).
	B3 Val d'Arpette Arette des Ecandies	• Rock falls • Rock falls	Duvernoy, CAF n°12, 588, 2005 Marjollin, CAF n°2, 2006
	B4 Col de Balme Croix de fer	• Explosion preceding the shaking • Rock falls	A. Riston, CAF, II, 38-39, 1906
	B5 Le Buet	• Rock fall	De Quervin, (1906).
	B6 Road Argentière-Le Tour	• 2-3 cm cracks along the road	CAF, II, 39, 1906
	B7 Chamonix	• Large crack in « Hotel de Genève » • Many cracks in the Railway station	Indicateur de la Savoie, August 19, 2005
	Martigny Grand Saint Bernard	• Fall of 2 chimneys • Plaster fall	Montandon, Revue études calamités, 1942

Table 1. Macroseismic effects in the epicentral areas of the April 29, 1905 earthquake: mainshock (1-a) and largest aftershock of August 13, 1905 (1-b). The numbers quoted An and Bn refer to the locations reported in Figure 2. Origin times t_0 of these two events are computed by making two hypotheses, Pg or Pn, on the nature of the reported P-wave arrival reported by Szirtes (1909), and rounding the value of t_0 to the minute (U.T. time).

.	*Station*	*Comp.*	T_0 *s*	α	*V*	*pol.*	*drum mm/min*	Δ *km*	*Az.*	*A mm*	*T*	M_s
1	GTT	E	15.3	0.46	180	-	14.9	653	18°	13.5	10.0	5.5
2	GTT	N	15.7	0.46	200	-	14.9	653	18°	3.6	9.3	4.9
3	UPP	E	9.4	0.38	187	+	14.5	1690	21°	1.1	8.5	5.1
4	UPP	N	9.8	0.38	188	+	14.5	1690	21°	0.7	7.8	4.9

Table 2. Instrumental parameters and determination of M_s at two stations Göttingen (GTT) and Uppsala (UPP) from the E and N components of horizontal Wiechert instruments: T_0 free period, α damping factor, *V* magnification, *pol.* polarization of the instrument, *drum* speed of the smoke-paper recorder, Δ epicentral distance, *Az.* back azimuth, *A* maximum amplitude on the record, *T* period at maximum amplitude, M_s surface-wave magnitude. Parameters are from the station booknotes and polarities refer to the ground motion. Charlier and Van Gills (1953) report polarities referring to the mass motion, which are opposite to those given in the present table.

Mec #		*r*	ϕ [°]	δ [°]	λ [°]	*h* [km]	τ/2 [*s*]	*Mean* M_W	*m*	σ_{M_W}
		0.78	**130**	**90**	**190**	**5**	**1**	**5.1**	**0.67**	**0.1**
F1		0.77	130	90	190	10	1	5.1	0.70	0.2
		0.75	130	90	190	15	1	5.2	0.74	0.2
		0.80	**20**	**70**	**290**	**5**	**1**	**5.3**	**0.67**	**0.2**
F2		0.76	20	70	290	10	1	5.3	0.76	0.1
		0.72	20	70	290	15	1	5.3	0.81	0.1
		0.37	60	66	169	5	1	5.4	1.10	0.2
F3		0.32	60	66	169	10	1	5.4	1.16	0.2
		0.25	60	66	169	15	1	5.4	1.23	0.2
		0.76	40	70	90	5	1	5.5	0.82	0.1
F4		0.64	40	70	90	10	1	5.5	1.06	0.1
		0.58	40	70	90	15	1	5.5	1.12	0.1
		0.70	40	20	90	5	1	5.5	0.94	0.1
F5		0.63	40	20	90	10	1	5.5	1.04	0.0
		0.62	40	20	90	15	1	5.5	1.11	0.1

Table 3. Five focal mechanisms Fn (strike ϕ, dip δ, rake λ), three depths h, and half duration τ/2 are used for computing the seismic waveforms at Göttingen and Uppsala (see also figure 5). The overall correlation coefficient *r* between the theoretical and the recorded seismograms shows how well both sets of waveforms are fitted. M_w is the mean of the individual station-component magnitude M_w, and σ_{Mw} is the standard deviation around the mean. See text for details.

Sample name	Type	Rock type	Thickness (cm)	Surface strike and dip	Latitude (°N)	Longitude (°E)	Elevation (m asl)	Shielding correction	Quartz mass (g)	9Be added (mg)	10Be/9Be*	err	10BE conc (at/g qtz)	err#	Exposure age$ (yrs)	err
REM1	bedrock	quartz poor phillite	2	N130, 43E	45,99	6,92	2040	0.6438	2,1773	0,06819	1,23E-13	7,5E-15	256783	15775	15461	1619
REM3	bedrock	quartz vein	2	N45 25NW	45,99	6,92	2070	0.9649	50,283	0,7055	2,38E-13	1,2E-14	217150	10949	8587	845
REM4	bedrock	quartz vein	2	N35, 25SE	45,99	6,92	2068	0.9734	50,034	0,7473	2,8E-13	1,1E-14	273082	10728	10752	1003
REM5	bedrock	quartz vein	2	0	45,99	6,92	2060	0.9759	50,095	0,7249	2,12E-13	1,3E-14	198819	12192	7818	816

* AMS measurements were performed at LLNL in 2002 for REM1 and at PrimeLab in 2005 for REM3, 4 and 5. They were normalized with the KNSTD reference as defined for the CRONUS-Earth online calculator v2.2 for standards prepared in 2002 and 2005 from ICN solution (Nishiizumi et al, 2007; NIM-B v. 258, p. 403).

Error on the concentration is AMS error.

$ Age is Lal(1991)/Stone(2000) time-dependend production model calculated using the CRONUS-Earth online calculator (http://hess.ess.washington.edu/) version 2.2. Error on age is the external uncertainty that includes both error on the nuclide concentration and error of model age used.

Table 4. 10Be cosmogenic isotope dating result of glacially polished bedrock surfaces in the vicinity of the Remuaz fault, Aiguilles Rouges massif.

748 **Table captions**

749

750 **Table 1.** Macroseismic effects in the epicentral areas of the April 29, 1905 earthquake: main shock
751 (1-a) and the largest aftershock of August 13, 1905 (1-b). The numbers quoted An and Bn refer to
752 the locations reported in Figure 3. Origin times t_0 of these two events are computed by making two
753 hypotheses, Pg or Pn, on the nature of the reported P-wave arrival reported by Szirtes (1909), and
754 rounding the value of t_0 to the minute (U.T. time). References to documents not cited in the
755 reference list (CAF for Club Alpin Français journal, regional newspapers, archives…) are given in
756 the table.

757

758 **Table 2.** Instrumental parameters and determination of M_s at two stations Göttingen (GTT) and
759 Uppsala (UPP) from the E and N components of horizontal Wiechert instruments: T_0 free period, α
760 damping factor, V magnification, *pol.* polarization of the instrument, *drum* speed of the smoke-
761 paper recorder, Δ epicentral distance, *Az.* back azimuth, B maximum amplitude on the original
762 record, T period at maximum amplitude, M_s surface-wave magnitude. Parameters are from the
763 station book notes and polarities refer to the ground motion. Charlier & Van Gills (1953) report
764 polarities referring to the mass motion, which are opposite to those given in the present table.

765

766 **Table 3.** Five focal mechanisms Fn (strike ϕ, dip δ, rake λ), three depths h, and half duration $\tau/2$ are
767 used for computing the seismic waveforms at Göttingen and Uppsala (see also Fig. 6). The overall
768 correlation coefficient r between the theoretical and the recorded seismograms shows how well both
769 sets of waveforms are fitted. M_w is the mean of the individual station-component magnitude M_w,
770 and σ_{Mw} is the standard deviation around the mean. See text for details.

771

772 **Table 4.** ^{10}Be cosmogenic isotope dating result of glacially polished bedrock surfaces in the vicinity
773 of the Remuaz fault, Aiguilles Rouges massif.

774

775

776 **Figure captions**

777

778 **Fig. 1.** Seismotectonic map of the northwestern part of the Alps near the Mont Blanc massif. Main
779 active faults from Thouvenot et al. (1998, 2003), Leloup et al. (2005), Armijo et al. (1986).
780 Epicentres of major events from SisFrance (2016) and ECOS-09 (2011). Green; macroseismic pre-
781 instrumental and yellow instrumental (M_w from SI-Hex, 2014; ECOS, 2011; and Rovida et al.
782 2011). 1996 and 1994 focal mechanisms are from Thouvenot et al. (1998) and Fréchet et al. (1996),

783 respectively. Mechanism for the 2005 event is from Fréchet al. (2011). RVSF: Rhône Valley-
784 Salvan fault or Vallorcine-Valais shear zone; CMBT: Courmayeur – Mont Blanc back thrust;
785 MBSZ: Mont Blanc shear zone. AB: cross-section line of Figure 6.
786
787 **Fig. 2.** Instrumental seismicity map for the period 1984-2008 from the ECOS-09 catalogue (Fäh et
788 al. 2011). Black rectangle outlines Figure 3. RF for Remuaz Fault trace, other fault traces are
789 labelled as in Figure 1.
790
791 **Fig. 3.** Locations of the best-documented macroseismic effects of the April 29 (A1 to A10 in red)
792 and August 13, 1905 (B1 to B7 in blue) events (for details see Table 1). E1 and E2 are the
793 macroseismic epicentres reported by SisFrance (2016) for the April 29 and August 13 events,
794 respectively. E3 shows the epicentre of the Vallorcine, September 8, 2005 earthquake (Fréchet et al.
795 2011). RF for the location of the steep Remuaz Fault scarp. Background map from the « Chamonix-
796 Sixt » 1:60,000 map (Vallot 1939). Grey dotted line is the trace of cross section A-A' of Figure 6
797 (see Fig. 1 for location).
798
799 **Fig. 4.** April 29, 1905 earthquake: partial collapse of a house in La Joux near Argentière (coll. Jules
800 et Michel Payot; Cuenot, 2015). For location see A5 in Figure 3.
801
802 **Fig. 5.** Argentière/Planet landslide shown by the red arrow, for location see A2-3 in Figure 3. View
803 looking to the NE from the Argentière railway station, a short time after it was built in 1906. The
804 spring, which appeared after the April 29, 1905 earthquake, was located at the foot of the landslide
805 area (coll. J.P. Gide; Gide and Banaudo 1998).
806
807 **Fig. 6.** Structural section A-A' across the Aiguiles Rouges and Mont Blanc massifs (see location in
808 Fig. 1) (modified from Leloup et al. 2005). Hypocentres of the two 1994 and 2005 earthquakes are
809 projected into the section and into corresponding structures. F1 to F5 indicate the various potential
810 fault zones tested in the text of section 4.3. F1 is a theoretical focal mechanism giving the best fit to
811 the seismic waveforms (see Table 3), F2 corresponds to the Remuaz fault and F3 to the fault
812 activated by the 2005 Vallorcine earthquake.
813
814 **Fig. 7.** Aerial view of the narrow N60° trending fault break in the steep northeastern flank of Gros
815 Nol (2458m) located at the southwestern end of the Vallorcine-Valais fault zone (tip of the
816 aftershock area of Vallorcine 2005 M_w=4.7 earthquake, Frechet et al., 2011). Bedrock break
817 predates the Vallorcine 2005 main shock as evidenced in October 2005 and 1973 photos taken from

818 the point shown by the red star.
819
820 **Fig. 8.** View of the Remuaz scarp along the eastern edge of the Aiguilles Rouges massif. The scarp
821 is outlined by a clear slope break and topographic step across the massif, and locally by ponding
822 (Goliet pond) and by a freshly striated exhumed basal strip (striations) (Alasset 2005).
823
824 **Fig. 9.** Left: aerial view of northeastern Aiguilles Rouges massif in the vicinity of Col des Montets.
825 In red, trace of Remuaz fault, which tends to disappear under late glacial morain deposits. Right:
826 topographic cross sections along the lines ab and cd perpendicular to the mean strike of Remuaz
827 fault. The fault zone was entirely covered by ice during the Last Glacial Maximum. The fault scarp
828 is a 40 to 60 m-high step clearly visible in the landscape. Outcropping striated scarp is only visible
829 to the north in the steepest slope of valley wall (star on the aerial view, section a-b). Inset: lower
830 hemisphere stereoplot of strike and dip of striated normal fault plane (in red) together with the rake
831 of the striations (red arrow). Strike and dip of steepest local slope is shown in black.
832
833 **Fig. 10.** a) Striations observed locally at the base of the Remuaz fault scarp (red rectangle). b) Steep
834 striations (pitch of 60°) that are clearly not glacial in origin. c) Along a length of 40 m the 20 cm
835 base of the scarp looks rejuvenated and devoid of lichens. d) Continuity of striations within a 1.5 m-
836 deep pit at the foot of the Remuaz fault scarp.
837
838 **Fig. 11.** a) Examples of "roche moutonnée" in the hangingwall of the Remuaz fault with clear
839 glacial striations. b) Close-up of a quartz-vein sample (to the right of hammer, sample REM3; Table
840 4) in striated bedrock.
841
842 **Fig. 12.** Göttingen horizontal records of the April 29, 1905 earthquake (Δ = 653 km). Love and
843 Rayleigh waves are dominant on the East and North component, respectively.
844
845 **Fig. 13.** Uppsala horizontal records of the April 29, 1905 earthquake (Δ = 1690 km).
846
847 **Fig. 14**. Records of the April 29 (upper trace) and August 13 (lower trace) drawn at the same scale
848 (Göttingen 1-ton Wiechert instrument, East component).
849
850 **Fig. 15.** Fits of the Göttingen (GTT) and Uppsala (UPP) filtered Wiechert records for the focal
851 mechanism of the Remuaz fault and a focal depth of 5 km (F2 in table 3). Recorded traces (in black)
852 and computed traces (in red) are normalized. Yellow zones indicate the time intervals where

853 computation of correlation r and misfit m are calculated. The Δ on the left is the epicentral distance,
854 A is the amplitude of the filtered signals (band-pass between 0.02 and 0.07Hz in GTT, 0.02 and
855 0.05Hz in UPP), w is the weight applied to each trace in the computation of r and m. Note that
856 because of the filtering process, amplitudes A are smaller than those of the original records shown
857 in Figures12 and 13.
858
859 **Fig. 16.** Variations of the misfit function *m* versus moment magnitude M_w for the five focal
860 mechanisms given in Table 3 and a focal depth of 5 km.

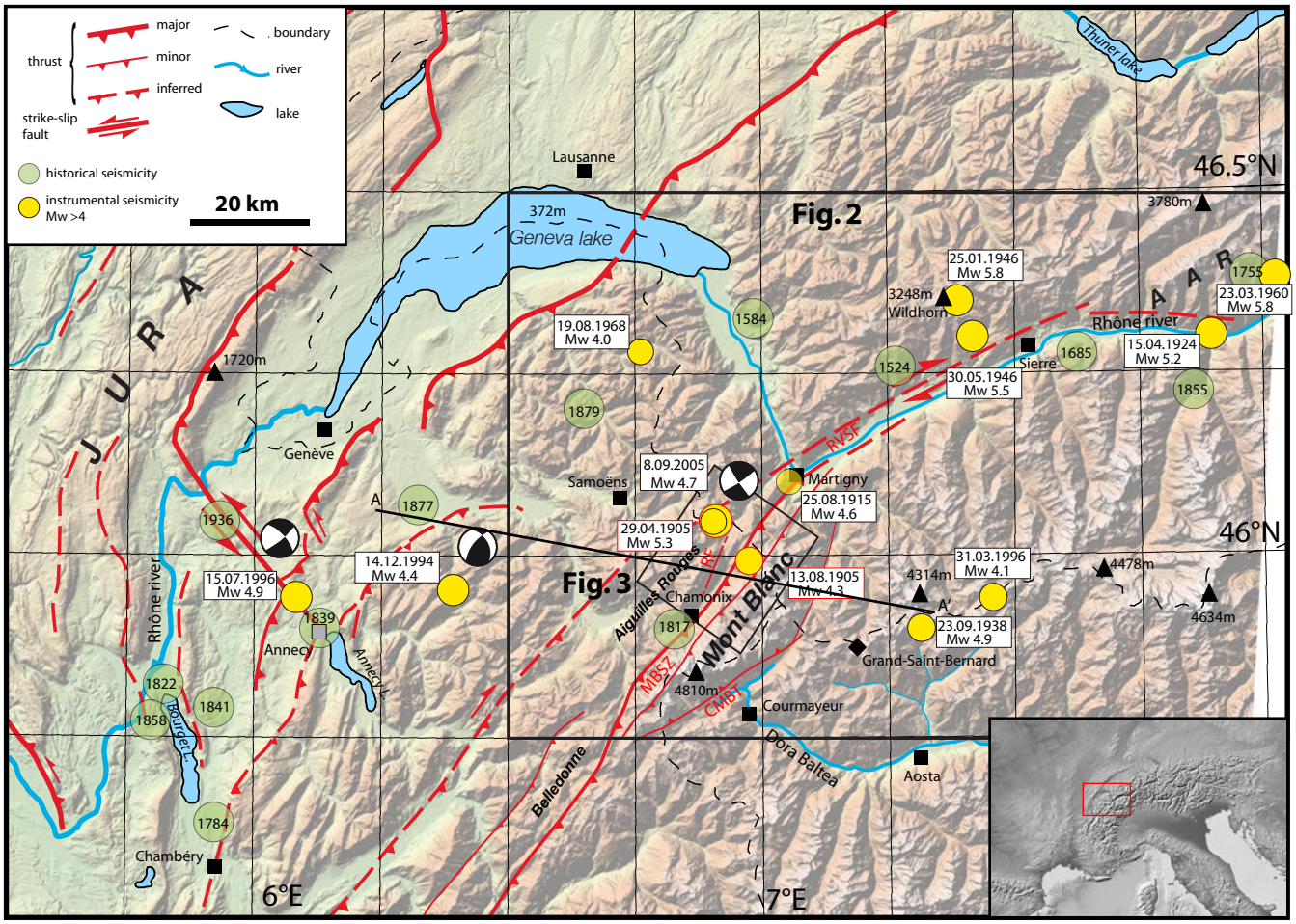
major
minor
inferred
thrust
strike-slip fault
boundary
river
lake
historical seismicity
instrumental seismicity Mw >4
20 km
Lausanne
Fig. 2
Fig. 3
372m
Geneva lake
Thuner lake
46.5°N
46°N
6°E
7°E
3780m
3248m
Wildhorn
25.01.1946 Mw 5.8
23.03.1960 Mw 5.8
Rhône river
15.04.1924 Mw 5.2
30.05.1946 Mw 5.5
Sierre
1755
1685
1524
1855
1584
19.08.1968 Mw 4.0
1720m
1879
Genève
JURA
AAR
RVSF
8.09.2005 Mw 4.7
Martigny
Samoëns
25.08.1915 Mw 4.6
29.04.1905 Mw 5.3
1877
1936
14.12.1994 Mw 4.4
15.07.1996 Mw 4.9
Rhône river
1839
Annecy
Annecy L.
1822
1858
1841
Bourget L.
1784
Chambéry
Aiguilles Rouges
RF
Chamonix
1817
Mont Blanc
13.08.1905 Mw 4.3
MBSZ
CMBT
4810m
Courmayeur
Grand-Saint-Bernard
4314m
31.03.1996 Mw 4.1
23.09.1938 Mw 4.9
4478m
4634m
Dora Baltea
Aosta
Belledonne

Figure 1

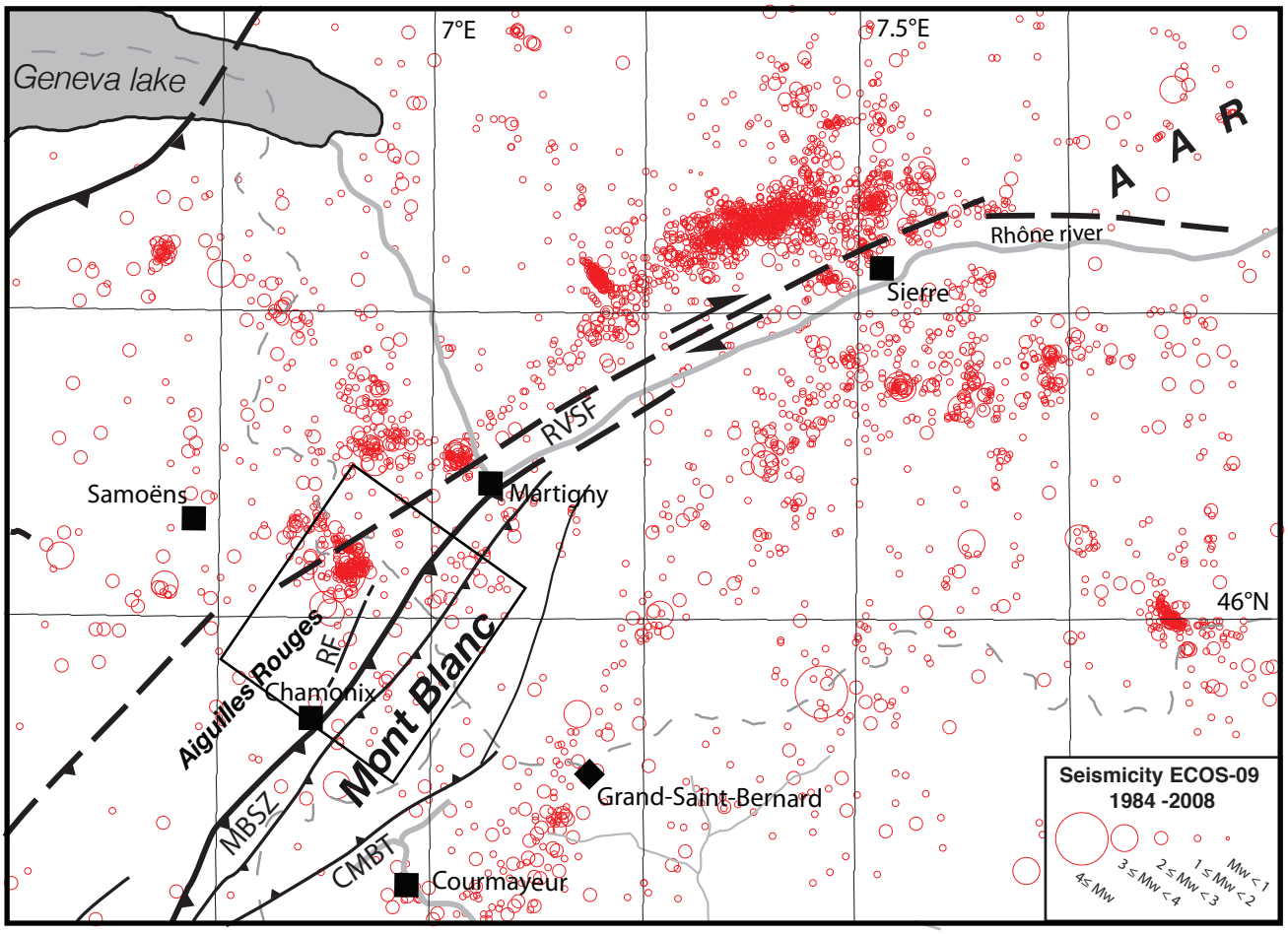
Geneva lake
7°E
7.5°E
A A R
Rhône river
Sierre
RVSF
Martigny
Samoëns
46°N
Aiguilles Rouges
RF
Chamonix
Mont Blanc
MBSZ
CMBT
Grand-Saint-Bernard
Courmayeur
Seismicity ECOS-09
1984 -2008
Mw < 1
1 ≤ Mw < 2
2 ≤ Mw < 3
3 ≤ Mw < 4
4 ≤ Mw

Figure 2

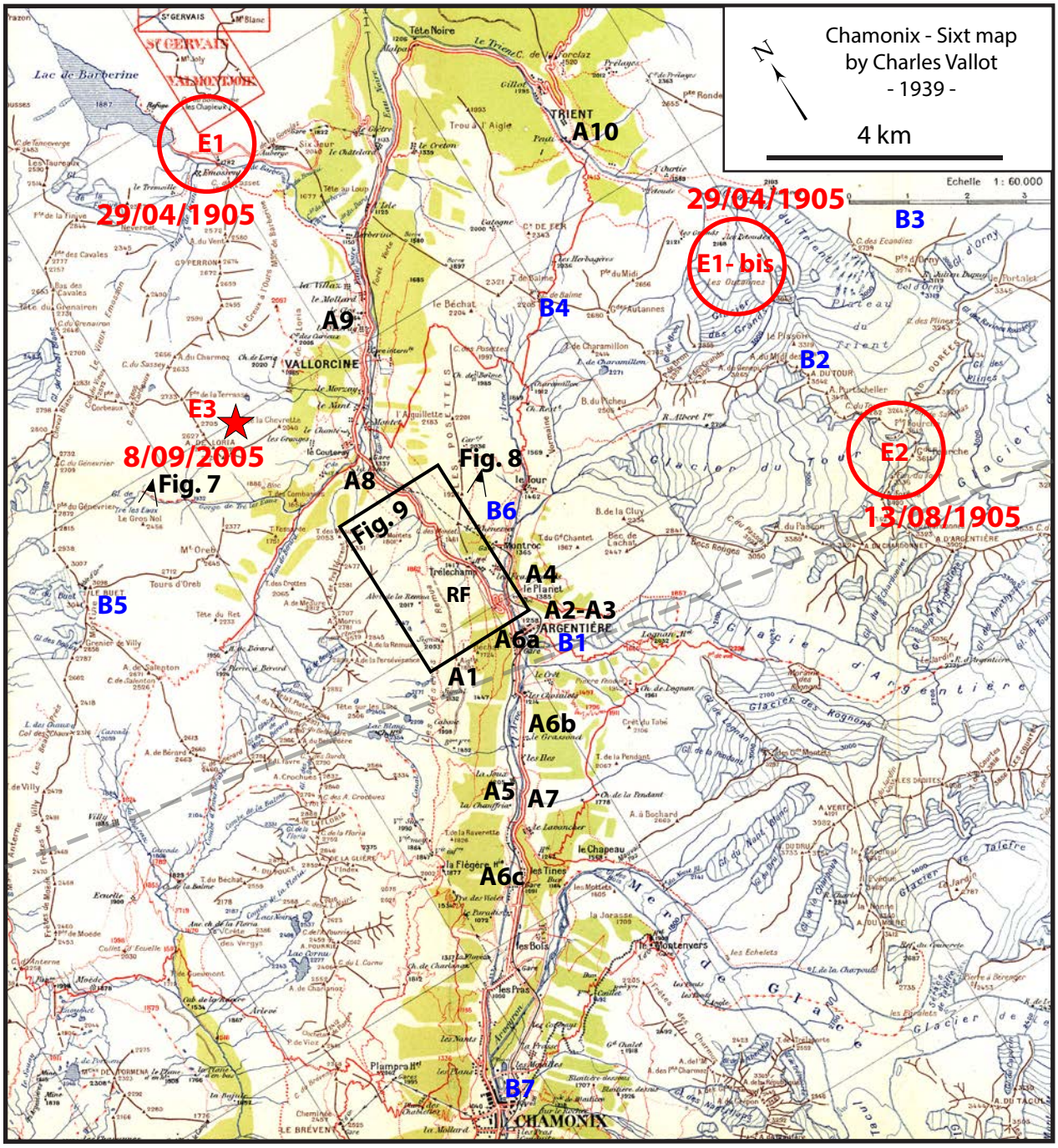
Chamonix - Sixt map
by Charles Vallot
- 1939 -
4 km
Echelle 1 : 60.000
E1
29/04/1905
E1- bis
29/04/1905
B3
E2
13/08/1905
E3
8/09/2005
Fig. 7
Fig. 8
Fig. 9
A8
A9
A10
B1
B2
B4
B5
B6
B7
A1
A2-A3
A4
A5
A6a
A6b
A6c
A7
RF
VALLORCINE
CHAMONIX
TRIENT
ARGENTIÈRE

Figure 3

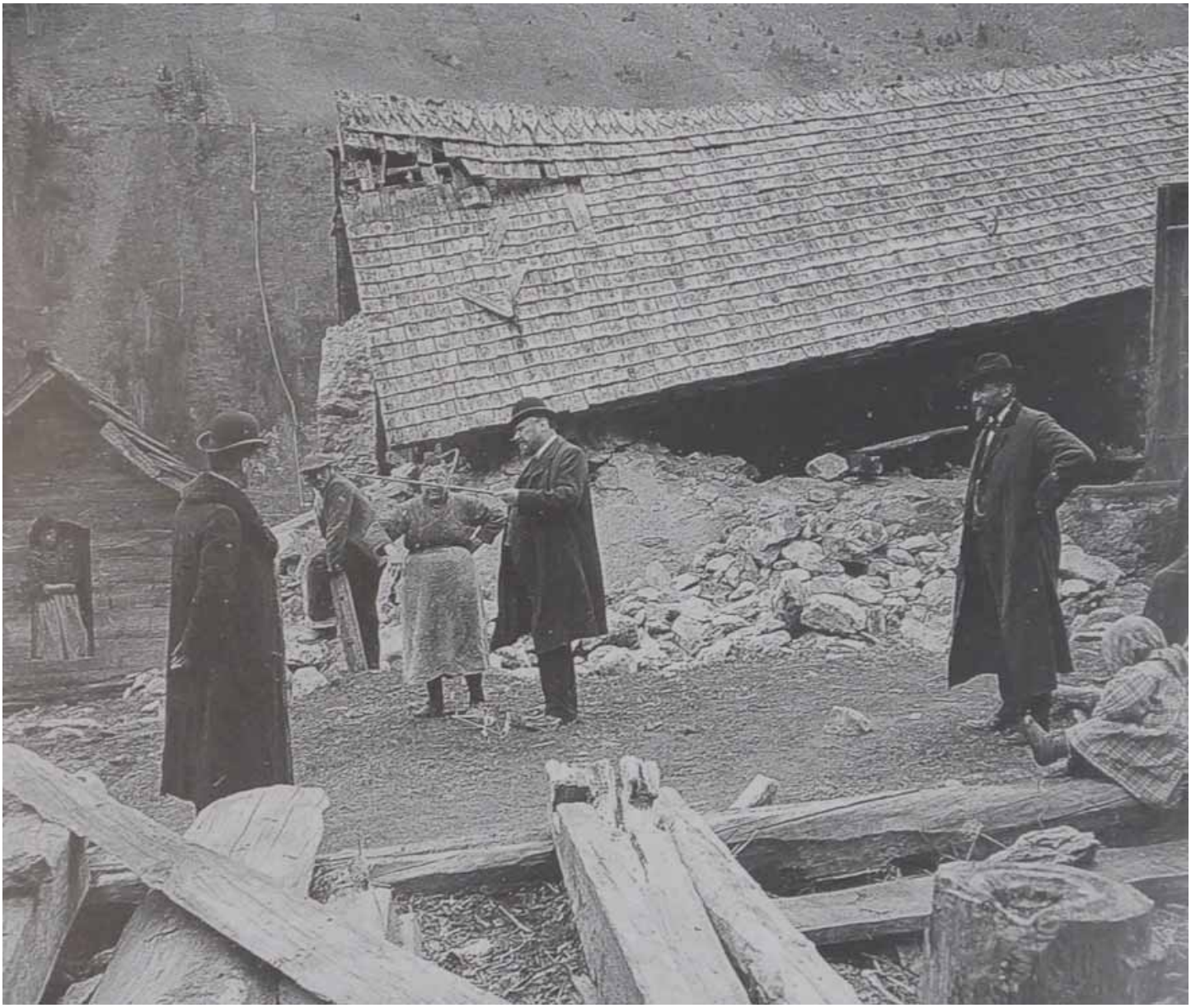

Figure 4

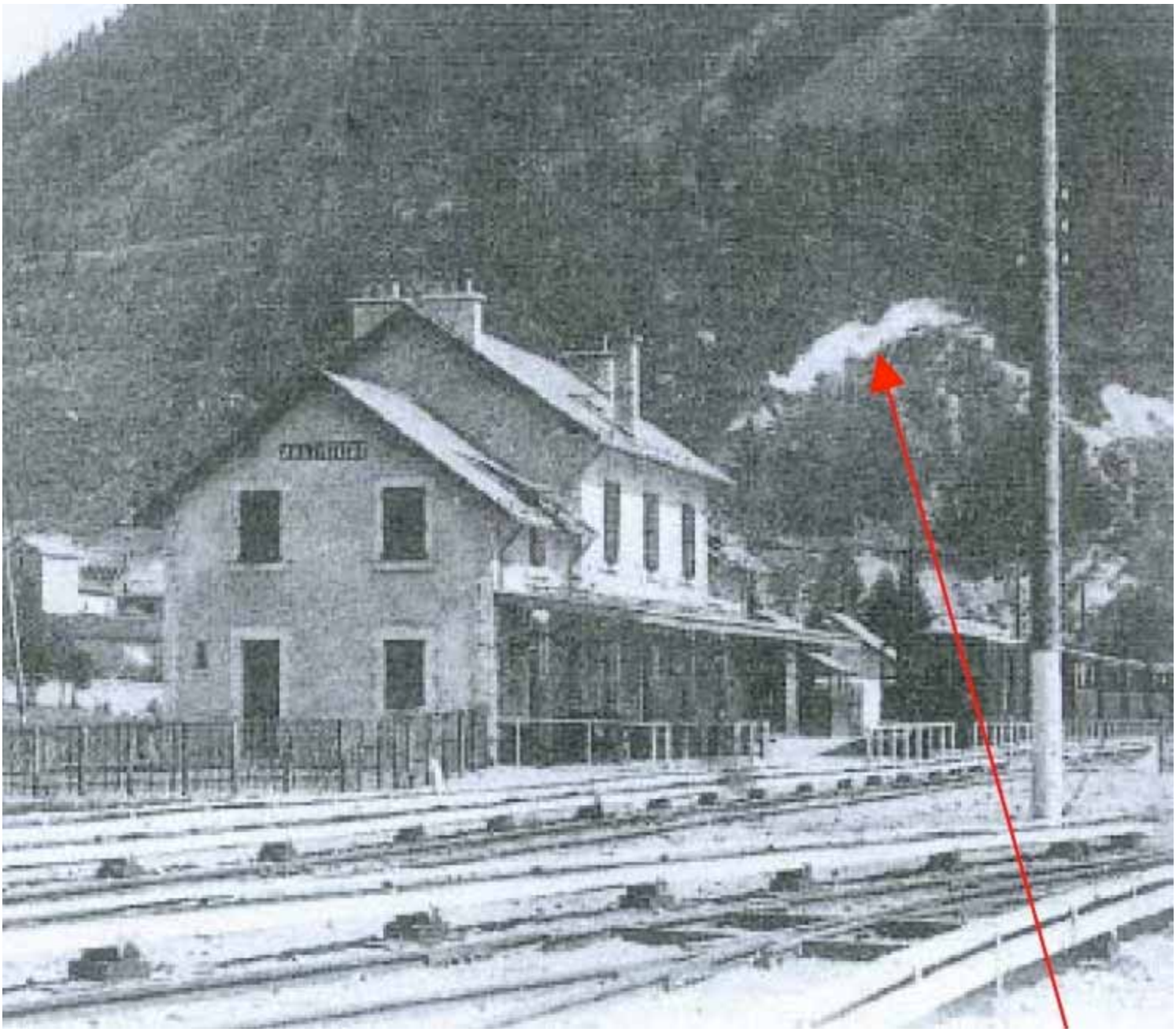

Figure 5

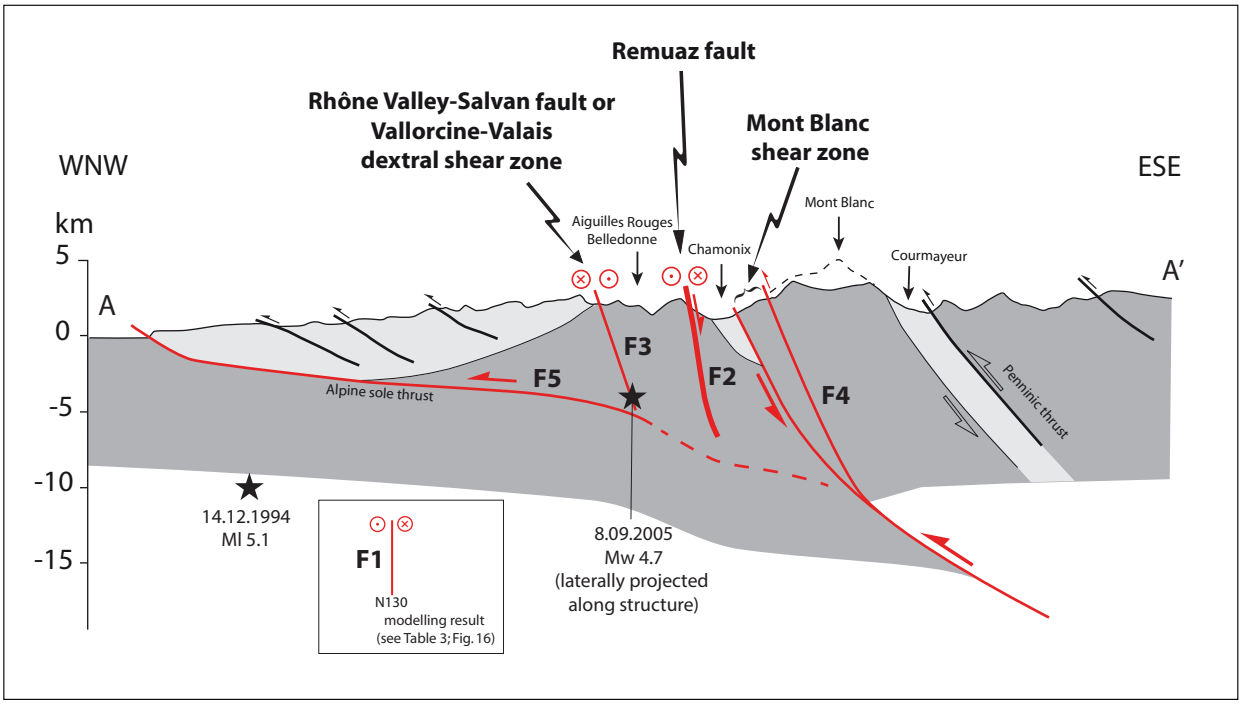
Remuaz fault
Rhône Valley-Salvan fault or
Vallorcine-Valais
dextral shear zone
Mont Blanc
shear zone
WNW
ESE
km
5
0
-5
-10
-15
A
A'
Aiguilles Rouges
Belledonne
Chamonix
Mont Blanc
Courmayeur
F1
F2
F3
F4
F5
Alpine sole thrust
Penninic thrust
14.12.1994
Ml 5.1
8.09.2005
Mw 4.7
(laterally projected
along structure)
N130
modelling result
(see Table 3; Fig. 16)

Figure 6

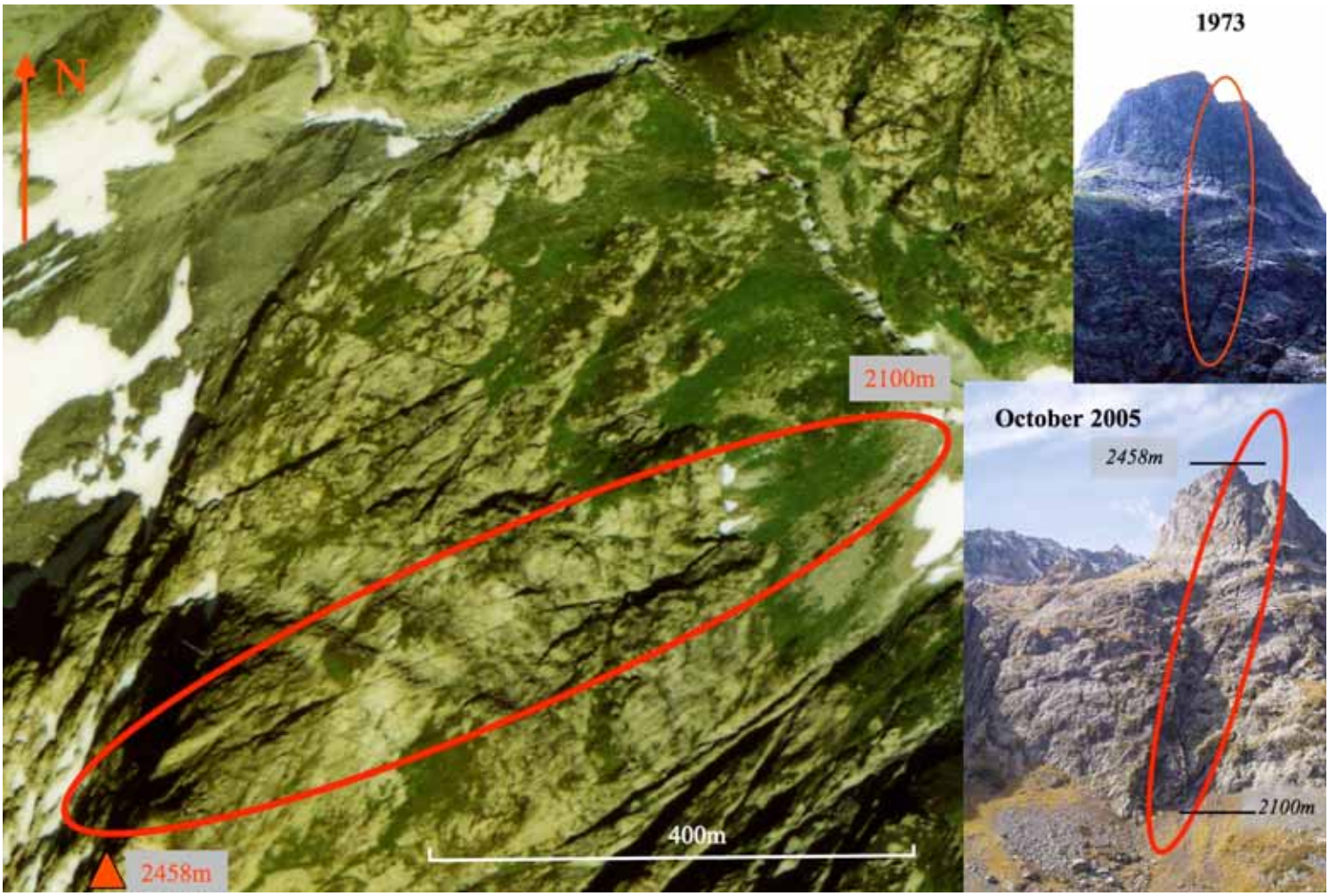

Figure 7

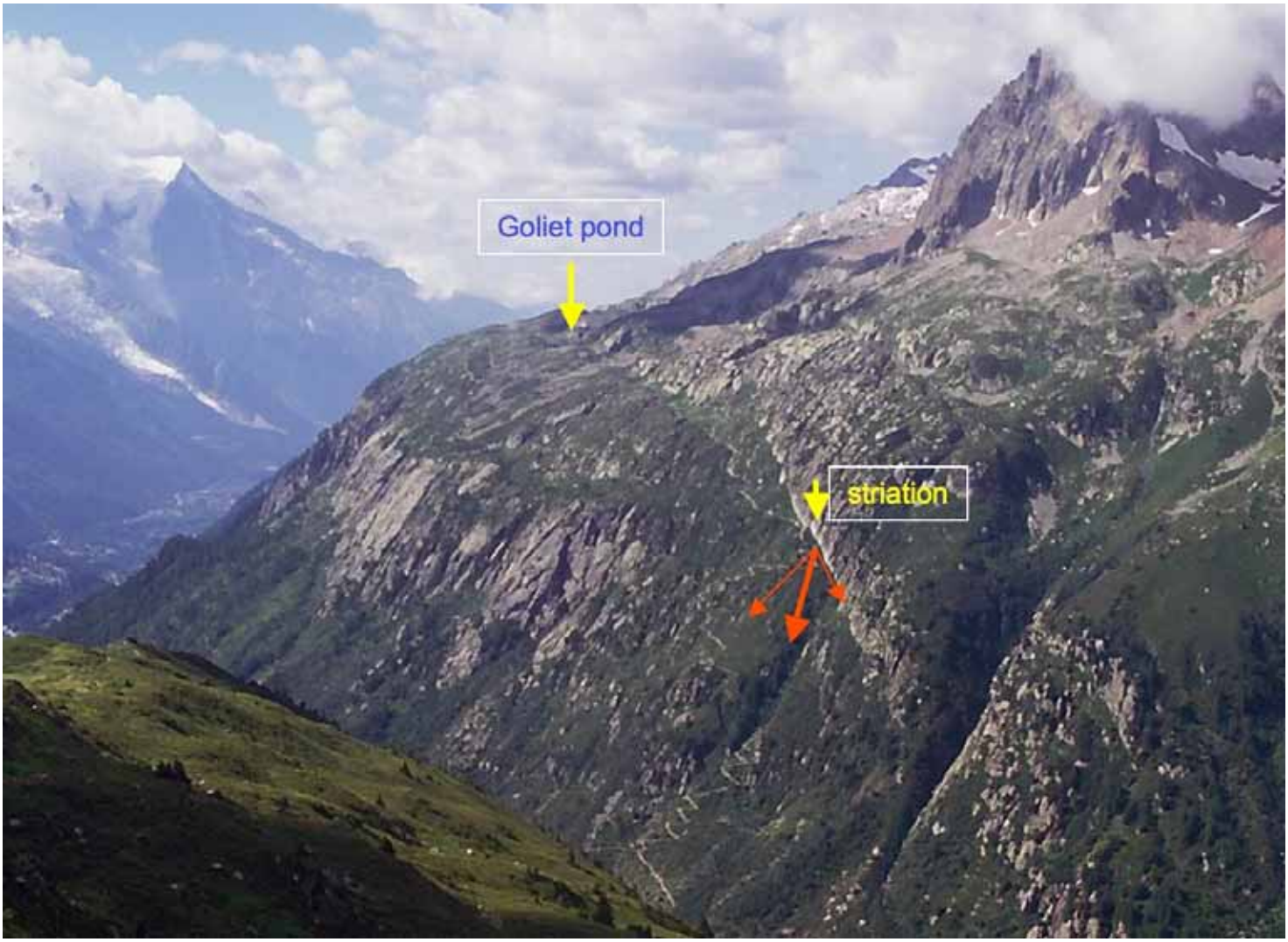

Figure 8

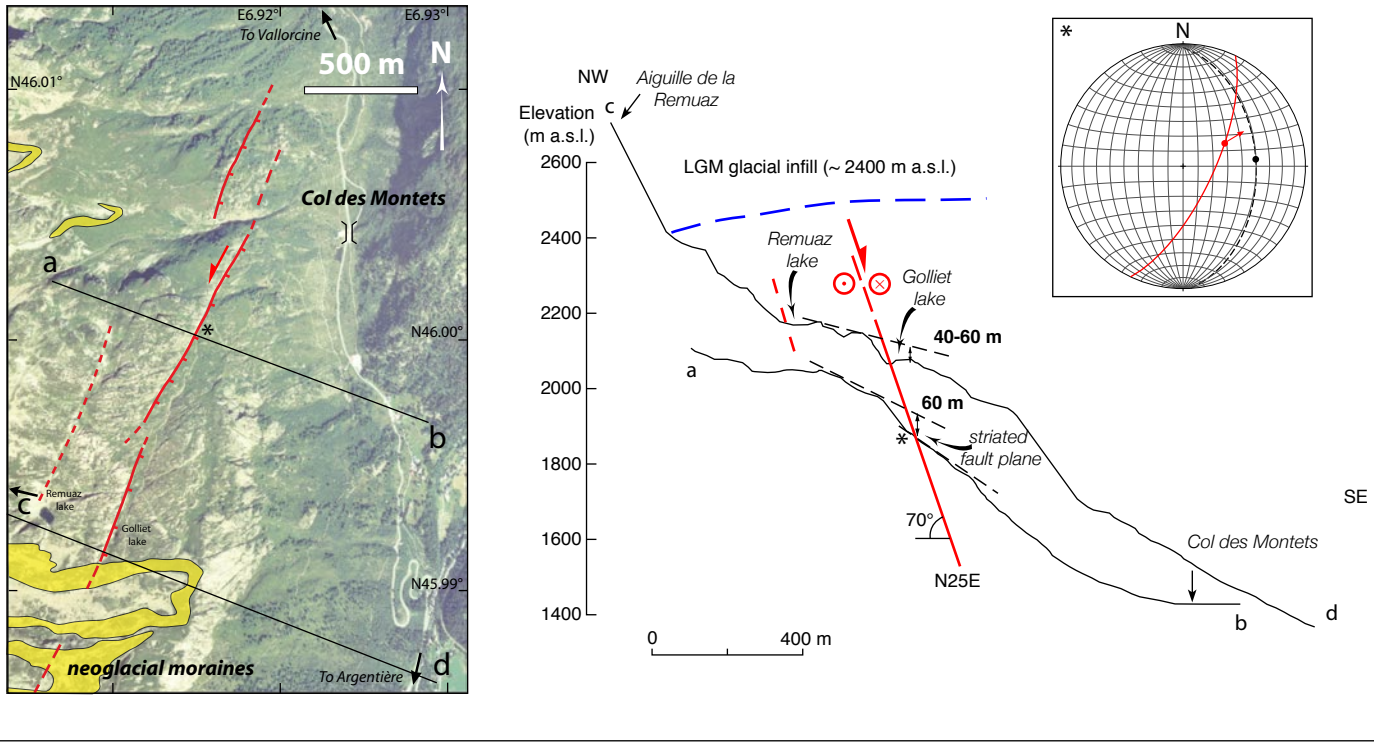
E6.92°
E6.93°
To Vallorcine
500 m
N
N46.01°
Col des Montets
a
N46.00°
b
c
Remuaz lake
Golliet lake
N45.99°
neoglacial moraines
To Argentière
d
NW
Aiguille de la Remuaz
Elevation (m a.s.l.)
c
LGM glacial infill (~ 2400 m a.s.l.)
2600
2400
2200
2000
1800
1600
1400
Remuaz lake
Golliet lake
40-60 m
a
60 m
striated fault plane
70°
N25E
SE
Col des Montets
b
d
0
400 m
N

Figure 9

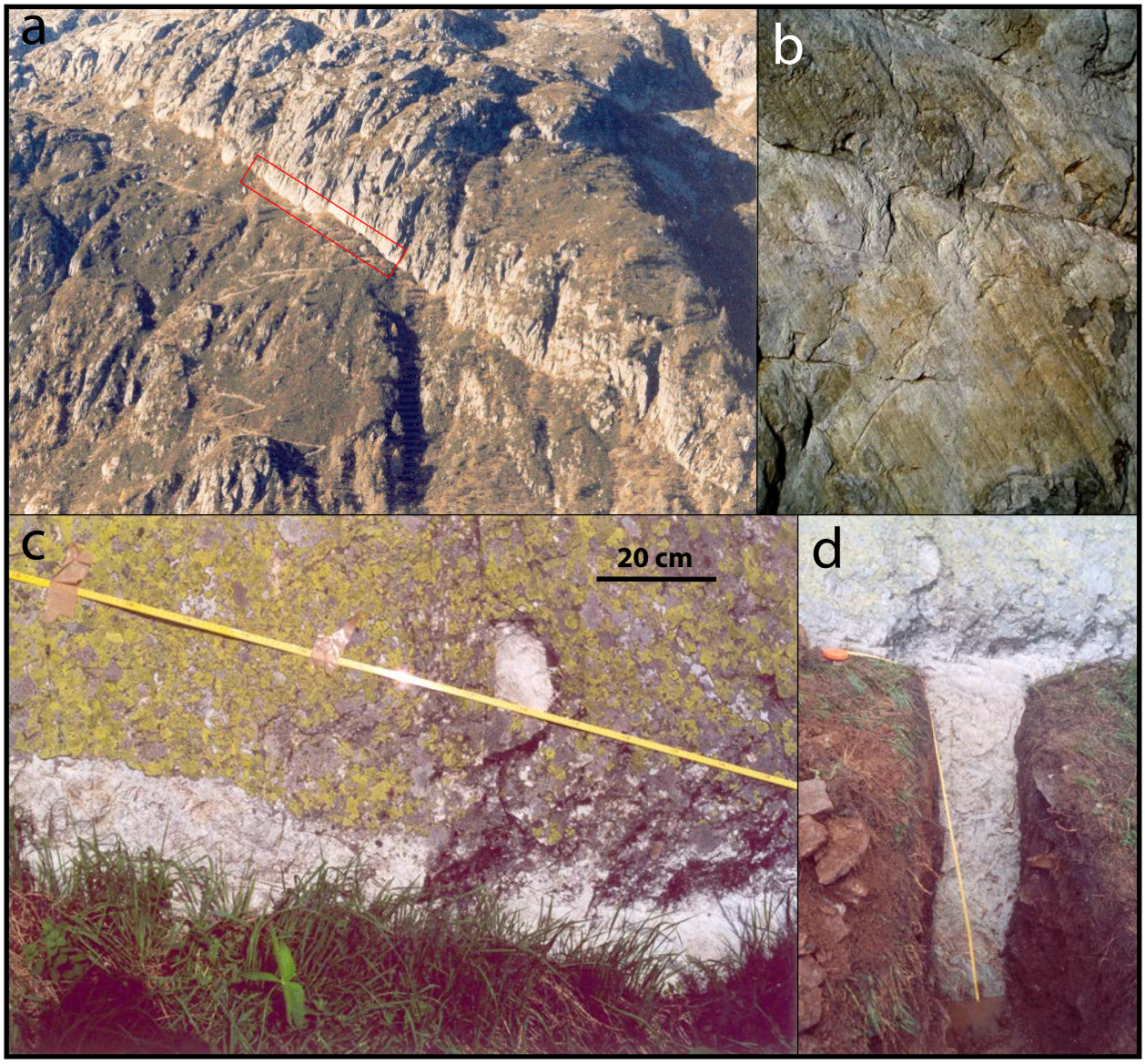

Figure 10

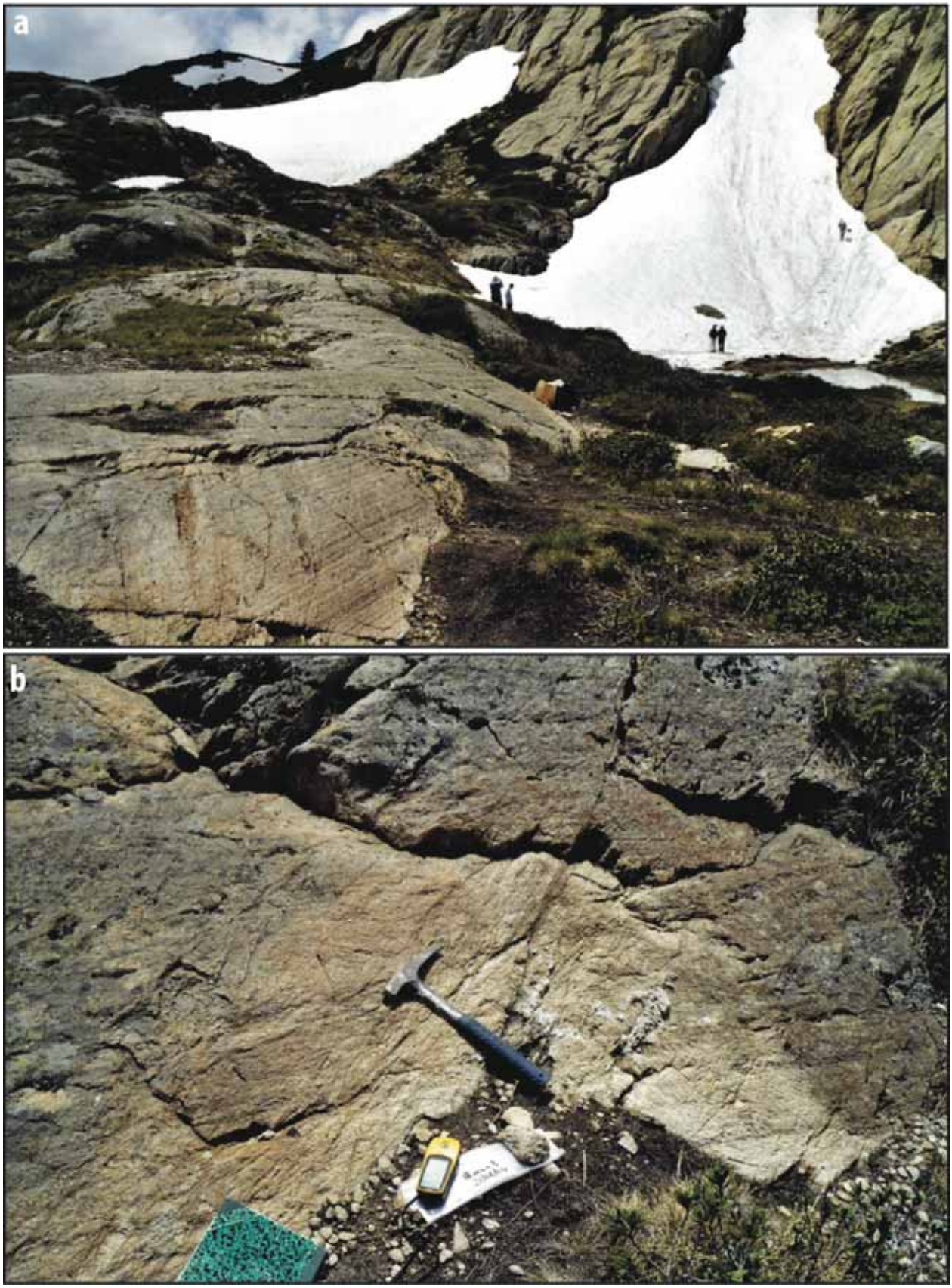

Figure 11

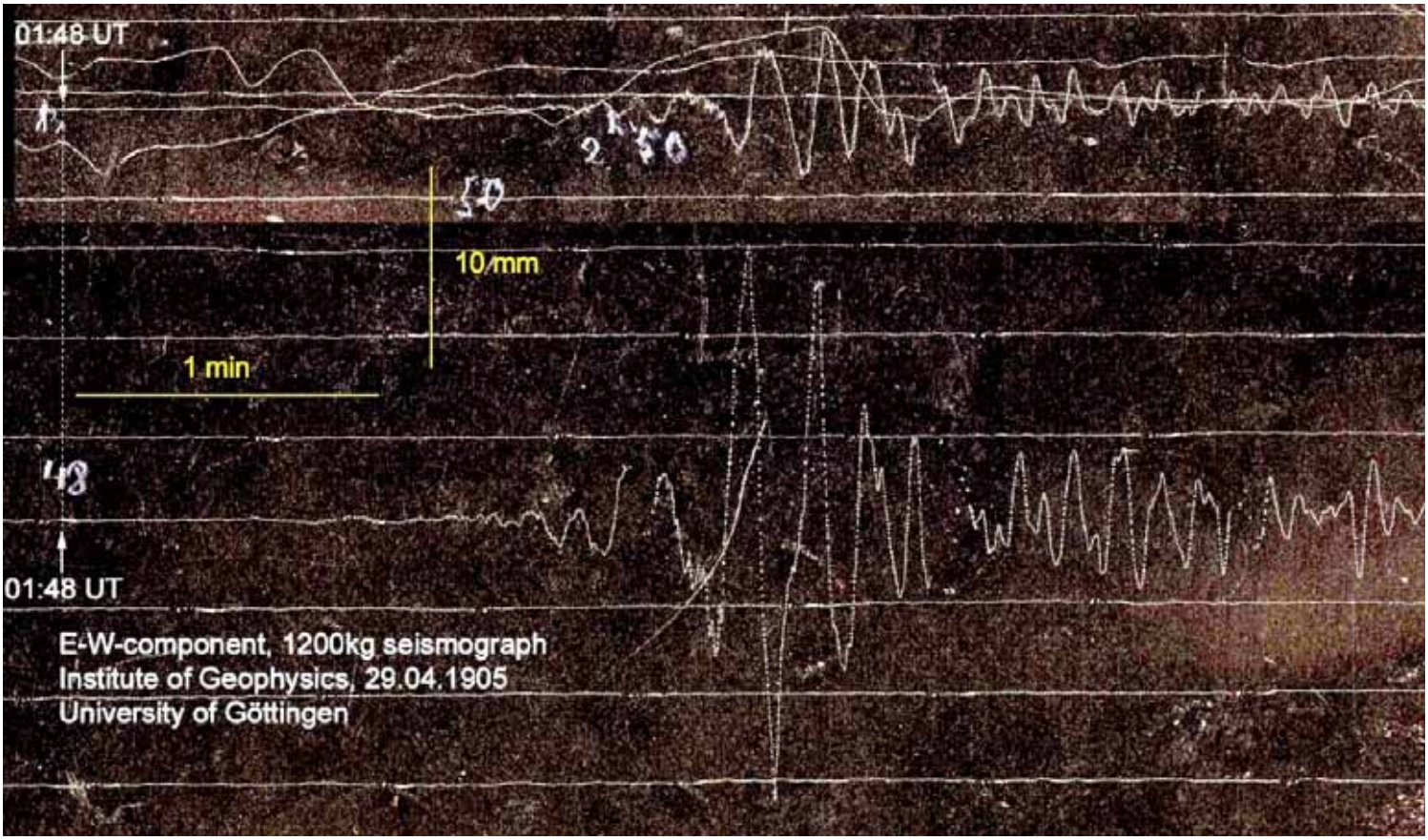
01:48 UT
10 mm
1 min
01:48 UT
E-W-component, 1200kg seismograph
Institute of Geophysics, 29.04.1905
University of Göttingen

Figure 12

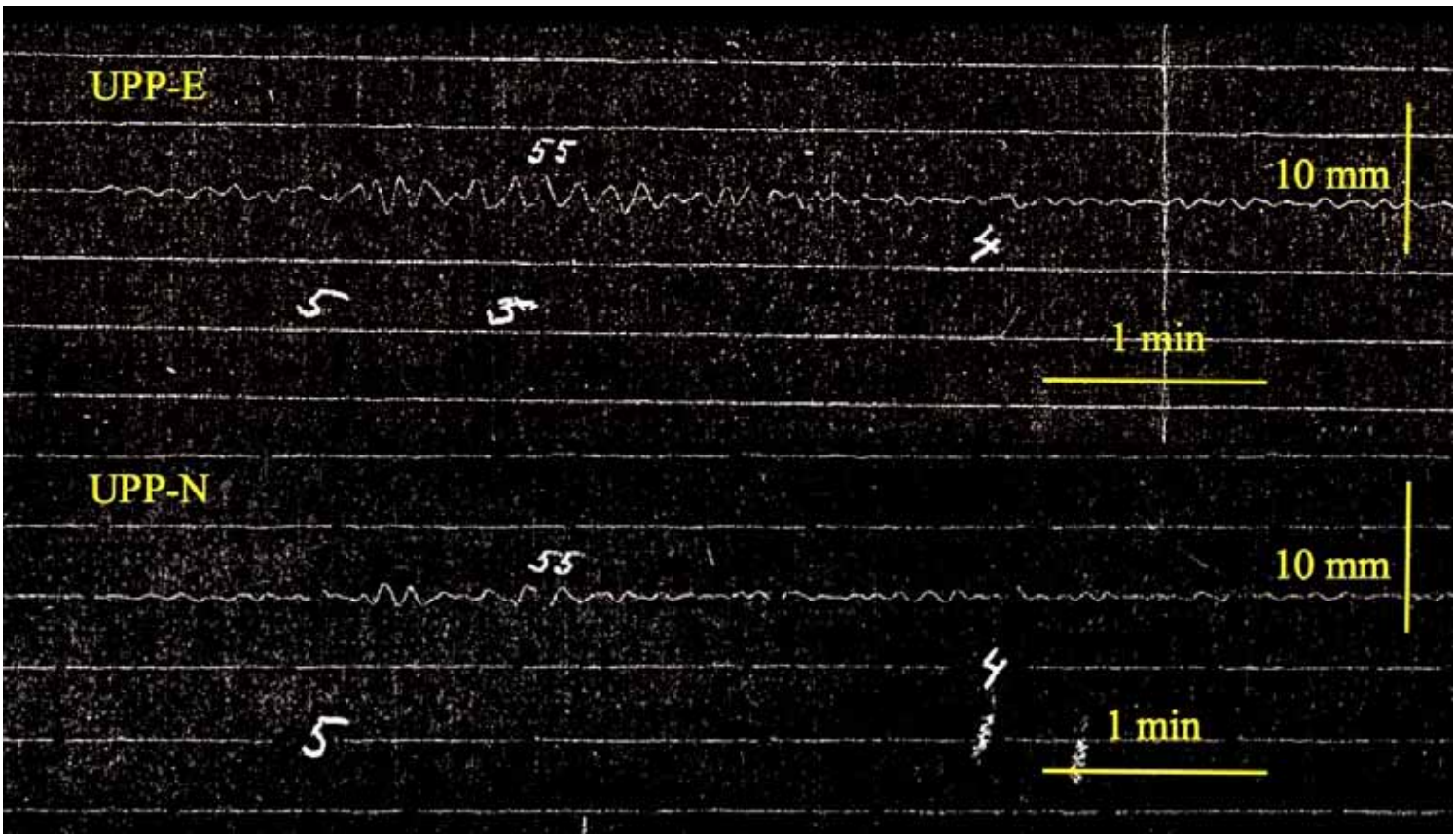

Figure 13

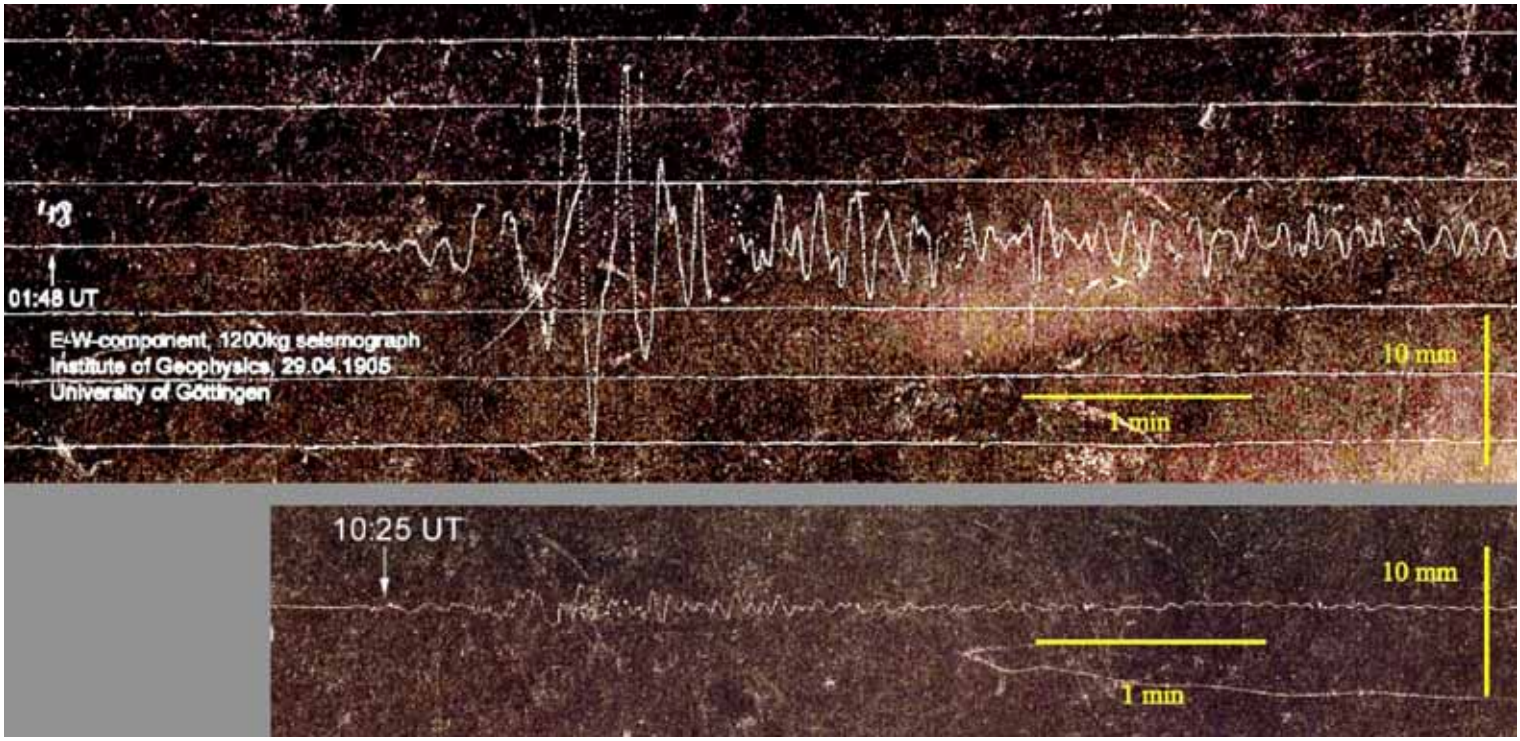
01:48 UT
E-W-component, 1200kg seismograph
Institute of Geophysics, 29.04.1905
University of Göttingen
10 mm
1 min
10:25 UT
10 mm
1 min

Figure 14

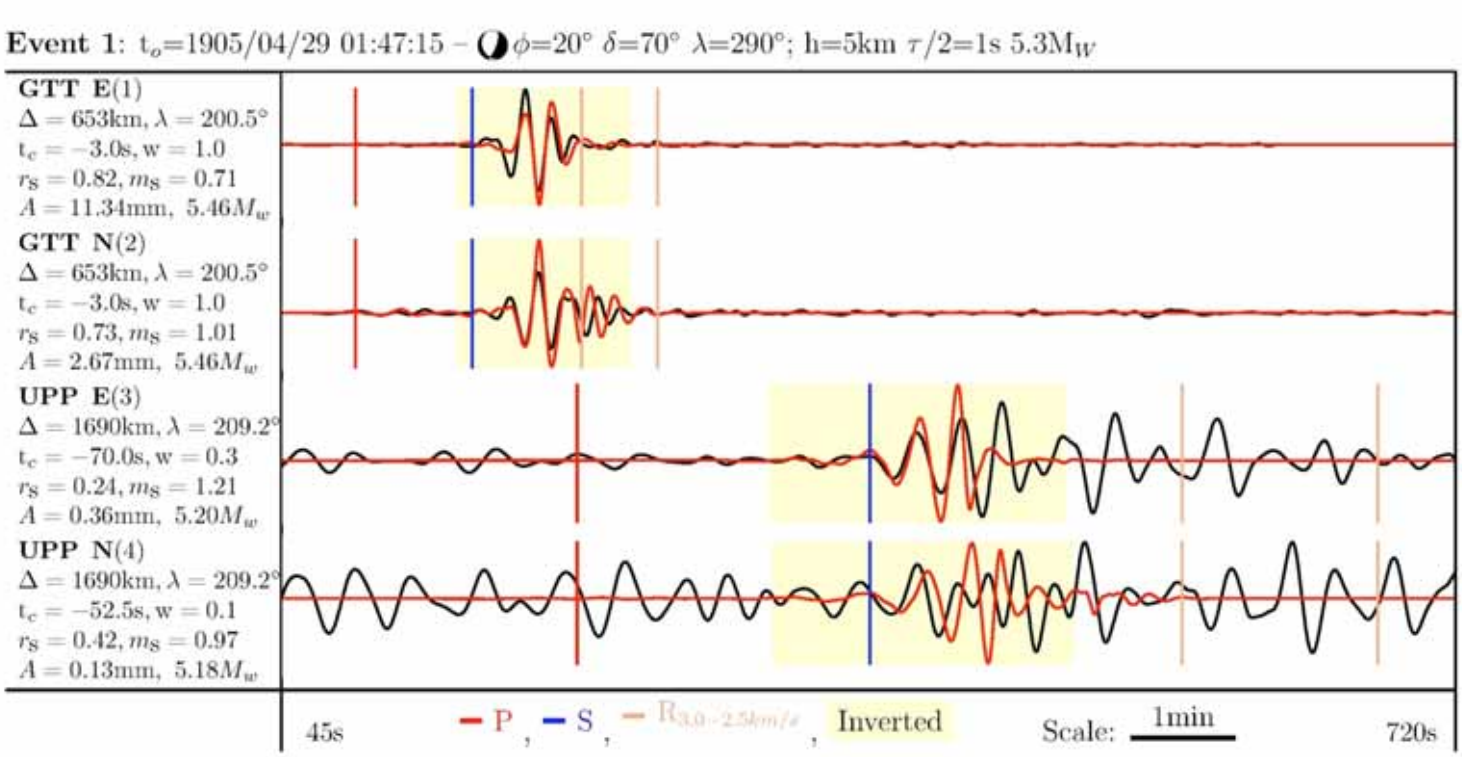
Event 1: t$_o$=1905/04/29 01:47:15 – ϕ=20° δ=70° λ=290°; h=5km τ/2=1s 5.3M$_W$
GTT E(1)
Δ = 653km, λ = 200.5°
t$_c$ = −3.0s, w = 1.0
r_S = 0.82, m_S = 0.71
A = 11.34mm, 5.46M_w
GTT N(2)
Δ = 653km, λ = 200.5°
t$_c$ = −3.0s, w = 1.0
r_S = 0.73, m_S = 1.01
A = 2.67mm, 5.46M_w
UPP E(3)
Δ = 1690km, λ = 209.2°
t$_c$ = −70.0s, w = 0.3
r_S = 0.24, m_S = 1.21
A = 0.36mm, 5.20M_w
UPP N(4)
Δ = 1690km, λ = 209.2°
t$_c$ = −52.5s, w = 0.1
r_S = 0.42, m_S = 0.97
A = 0.13mm, 5.18M_w
45s
P , S , R3.0 - 2.5km/s , Inverted
Scale: 1min
720s

Figure 15

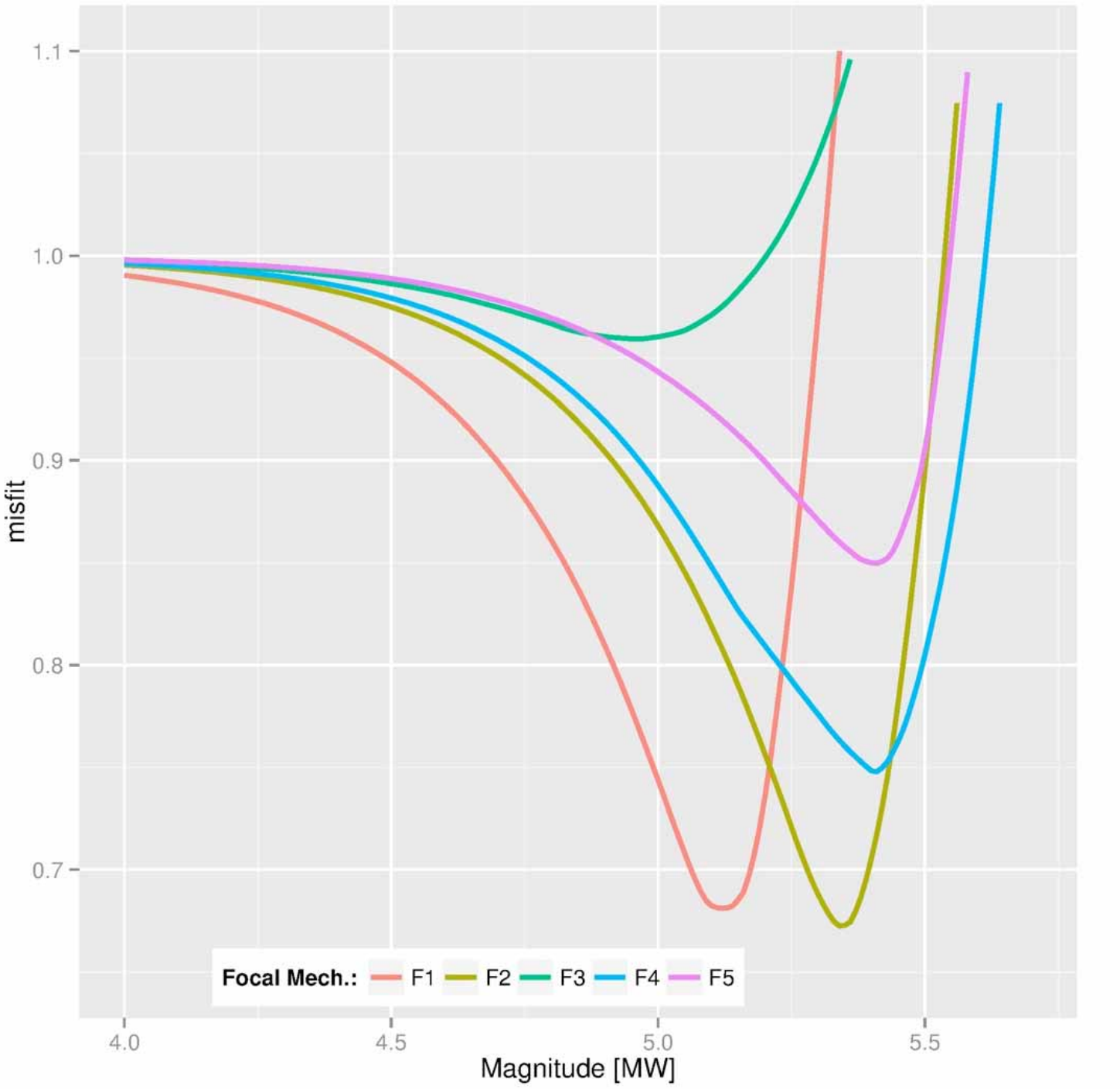
1.1
1.0
0.9
0.8
0.7
misfit
Focal Mech.:
F1
F2
F3
F4
F5
4.0
4.5
5.0
5.5
Magnitude [MW]

Figure 16